Available online at www.sciencedirect.com
SCIENCE DIRECT
Journal of Photochemistry and Photobiology A: Chemistry 176 (2005) 15–38
Journal of Photochemistry and Photobiology A:Chemistry
www.elsevier.com/locate/jphotochem

Spectroscopic studies of the I_2/O_3 photochemistry Part 1: Determination of the absolute absorption cross sections of iodine oxides of atmospheric relevance

Juan Carlos Gómez Martín *, Peter Spietz, John P. Burrows

Institute of Environmental Physics, University of Bremen, PO Box 330440, 28334 Bremen, Germany

Available online 28 October 2005

Abstract

Multichannel time resolved absorption spectroscopy has been coupled with flash photolysis of mixtures of molecular iodine and ozone to study the spectra and determine absorption cross sections of iodine oxides. Simultaneously, the behaviour of the iodine atoms has been measured by atomic resonance spectroscopy. To separate overlapping molecular absorptions, multivariate analysis techniques have been used to yield the optical density versus time curve at an optimal wavelength for each individual molecular absorber.

After the initial photolysis of I_2 and some O_3, it is assumed that the number of iodine atoms contained in the chemical system is invariant *in time* and that the individual optical densities of *all* the relevant species are observed. The solution of the resultant over-determined system of linear equations yields the absolute absorption cross sections of the iodine containing molecular species: ground state iodine monoxide, IO($X^2\Pi_{3/2}$, $v''=0$), vibrationally excited iodine monoxide, IO($X^2\Pi_{3/2}$, $v''>0$), ground state iodine dioxide, OIO($^2B_1$), and the spectra of three other iodine oxides, some of which have been observed for the first time in this study. One of these oxides has been tentatively assigned to I_2O_2, and possible assignments of the other two have been discussed.

The values of absolute absorption cross sections for selected vacuum wavelengths at 298 K were determined to be: $\sigma_{IO(4\leftarrow0)}(427.2\,nm) = (3.5 \pm 0.3) \times 10^{-17}\,cm^2$, $\sigma_{IO(3\leftarrow1)}(459.3\,nm) = (4.5 \pm 0.5) \times 10^{-17}\,cm^2$, $\sigma_{IO(1\leftarrow2)}(484.9\,nm) = (6.0 \pm 0.5) \times 10^{-17}\,cm^2$, $\sigma_{OIO(0,5,1\leftarrow0,0,0)}(549.3\,nm) = (1.3 \pm 0.3) \times 10^{-17}\,cm^2$ and for an up to now unidentified higher iodine oxide $\sigma(356\,nm) \geq (7.8 \pm 1.2) \times 10^{-19}\,cm^2 \times I\,atom^{-1}$. The spectral resolution of the resultant absorption cross sections is 0.12 nm FWHM in case of IO and 0.35 nm FWHM in case of OIO. Previous determinations of these absorption cross sections have been reviewed.

Keywords: Molecular absorption spectroscopy; Absolute absorption cross sections; Ozone-halogen chemistry; Iodine oxides

1. Introduction

As a result of the interest in stratospheric removal of ozone, many studies have investigated the halogen reactions of atmospheric significance. Simultaneously, an effort has been made to determine accurately the molecular parameters of halogen containing species.

A detailed knowledge about the role of chlorine and bromine species in atmospheric ozone chemistry already exists. In contrast, the role of iodine species is less well known. Gas phase iodine radicals have been a source of scientific interest over the last two decades as a result of their potential role in stratospheric and tropospheric ozone chemistry, and more recently because of their possible impact on aerosol formation and thereby on atmospheric radiative transfer. The works of Chameides et al. [1], Chatfield et al. [2], and Solomon et al. [3] provided an important impulse to the investigation of the kinetics and spectroscopy of key iodine containing species like IO and to their detection in the atmosphere. A product of this effort was the discovery of OIO (Himmelmann et al. [4]), which was subsequently suggested as a precursor to aerosol condensation nuclei (Cox et al. [5], Hoffmann et al. [6], O'Dowd et al. [7]). Field measurements have detected IO in the atmosphere (Wittrock et al. [8,9], Alicke et al. [10], Allan et al. [11], Saiz-López et al. [12]), further stimulating the detailed modelling of iodine chemistry (Vogt et al. [13], McFiggans et al. [14]). Recently OIO has been detected in the troposphere at night (Allan et al. [15], Saiz-López et al. [12]).

Iodine atoms are known to be released in the atmosphere by photolysis of iodocarbons of biogenic origin (Carpenter et al. [16]). The photolysis of biogenic I_2 has also been proposed as a

* Corresponding author. Tel.: +49 421 2182286; fax: +49 421 2184555.
E-mail address: jcgomez@iup.physik.uni-bremen.de (J. Carlos Gómez Martín).

1010-6030/$ – see front matter © 2005 Elsevier B.V. All rights reserved.
doi:10.1016/j.jphotochem.2005.09.024

source of I atoms (Saiz-López et al. [12]). In either case, the first step in iodine-catalysed O_3 destruction cycles is the reaction

$$I + O_3 \rightarrow IO + O_2 \quad (1)$$

Reactions that convert IO back to iodine atoms without O atom formation lead to catalytic O_3 loss. Chain propagation for the iodine-catalyzed ozone loss in the stratosphere is most likely by the reaction of IO with ClO and/or BrO. The current understanding is that the stratospheric ozone loss enhancement by iodine is of minor importance as a result of low IO concentrations, the rate constants for halogen coupling reactions at $T < 210$ K being slower than originally predicted, and a large yield of OClO from the reaction of ClO + IO (Salawitch [17], Rowley et al. [18] and references therein).

The IO self-reaction has been proposed as one of the most important reactions leading to catalytic ozone destruction in the troposphere

$$IO + IO \rightarrow I_2 + O_2 \quad (2a)$$

$$\rightarrow 2I + O_2 \quad (2b)$$

$$\rightarrow I + OIO \quad (2c)$$

$$\overset{M}{\leftrightarrow} I_2O_2 \quad (2d)$$

$I(^2P_J)$ atoms are generated directly by the IO self-reaction, and in daytime by the photolysis of I_2, resulting in additional consumption of O_3, and IO being regenerated. The photolysis of OIO, if it occurs, proceeds via

$$OIO \overset{h\nu}{\rightarrow} I(^2P_J) + O_2 \quad (3)$$

The photolysis of OIO to IO + $O(^3P)$ has been found to be small, with an upper limit for the quantum yield at 532 nm of 7×10^{-3} (Ingham et al. [19]). Therefore, the cycle of reactions (1–2–3) leads to ozone destruction and a large chain length. The atmospheric fate of OIO is currently under discussion (see [19–22]). A slow photolysis rate of OIO would result in smaller ozone catalytic chain length, and an enhancement of its potential to form aerosol nuclei. The irreversible accumulation of the two main products of the IO self-reaction (OIO and I_2O_2) has been proposed as the main cause for the iodine enrichment of aerosol [5–7].

A prerequisite for the quantitative atmospheric measurement of important iodine containing species by spectroscopic techniques is the determination in laboratory studies of their absorption cross sections (σs). Many field measurements use DOAS (differential optical absorption spectroscopy, see Platt [23] and references therein), which is based on a variant of the Beer–Lambert Law to obtain concentrations

$$I(\lambda, t) = I_0(\lambda, t) \exp(-Lc(t)\sigma(\lambda))$$

$$\Rightarrow a(\lambda, t) \equiv \ln\left(\frac{I_0(\lambda, t)}{I(\lambda, t)}\right) = Lc(t)\sigma(\lambda) \quad (i)$$

where $I_0(\lambda, t)$ and $I(\lambda, t)$ are, respectively the reference and the transmitted intensities, $a(\lambda, t)$ is the optical density (OD) or absorbance (the notation 'a' adopted here refers to "absorbance", although the preferred terminology is "optical density"), L the path length, $c(t)$ the concentration and $\sigma(\lambda)$ the absolute absorption cross section of the molecule. The determination of atmospheric photolysis rates depends also on the knowledge of the corresponding absorption cross section.

1.1. Previous studies of IO

The IO $A^2\Pi_{3/2} \leftarrow X^2\Pi_{3/2}$ subband system was first observed in 1937 by Vaidya [24] from its emission in a methyl iodide flame. In 1948 Coleman et al. [25] observed the same emission spectrum by using an oxyhydrogen flame to which iodine was added, thus supporting the assignment to IO. In 1958 Durie et al. [26] recorded the first absorption spectrum of IO in flash photolysis experiments. Also Durie et al. [27] photographed the methyl iodide flame bands and carried out rotational and vibrational analysis, which confirmed the spectral assignment to IO. Several authors have determined the absorption cross section at the band head and/or at the maximum of the $(4 \leftarrow 0)$ band of IO [28–34], denoted here as $\sigma_{IO}(4 \leftarrow 0)$. The results are summarized in Table 1 and show a relatively large variability.

A first explanation for such variability could be the selection of different wavelengths to determine σ_{IO}. Another cause could be the different spectral resolution employed, which affects both the value of the peak absorption and its wavelength position. Finally, the determination of the concentration of IO is also likely to be a significant source of bias. In general, the determination of σs is critically linked to the kinetic assumptions made in order to determine concentrations. All these sources of uncertainty are discussed in this work.

Three different sources of IO have been used in previous works to perform spectroscopic and kinetic studies of IO and the products of its self-reaction: namely reaction (1) and the two following reactions:

$$O(^3P) + I_2 \rightarrow IO + I(^2P_J) \quad (4)$$

$$O(^3P) + CF_3I \rightarrow IO + CF_3 \quad (5)$$

Oxygen atoms, $O(^3P)$, and iodine atoms, $I(^2P_J)$, are produced by the photolysis of N_2O or O_3, and the photolysis of I_2,CH_3I or CH_2I_2, respectively.

In previous studies two ways have been used to determine the absorption cross section of IO. In the first approach, the determination of IO absorption cross section requires an estimate of its concentration. This assumes the conservation of mass within the experiment. The concept is to equate the concentration of IO instantaneously produced to the concentration of one of its atomic precursors, or in other words, to consider quantitative conversion of I/O atoms to IO. Reaction (4) or (5) are in general preferred as sources of IO in the determination $\sigma_{IO}(4 \leftarrow 0)$ to reaction (1). This is because of more complex kinetics involved in systems based on reaction (1) and its slower rate coefficient. For systems using reaction (4) an approach based on the conser-

Table 1
Cross sections σ_{IO}(427.2 nm), σ_{OIO}(549.3 nm) and σ_Z

Reference	P (mbar)	T (K)	FWHM (nm)	$\sigma_{IO}(4 \leftarrow 0) \times 10^{17}$ (cm^2)		$\sigma_{OIO}(0,5,1 \leftarrow 0,0,0) \times 10^{17}$(cm^2) 459.2 nm (vac)	$\sigma_Z \times 10^{18}$ (cm^2) [λ (nm)]
				σ_{IO} [λ (nm)]	σ_{IO} at 427.2 nm (vac)		
Cox et al. [28]	1013	303	0.27	$3.1^{+2}_{-1.5}$ [426.9, air]	$(3.7^{+2.5}_{-1.9})$[a]	–	–
Jenkin et al. [29]	9–93	306	0.27	$>2.2 \pm 0.5$[b] [426.9, air]	$>(2.6 \pm 0.9)$[a]	–	–
Sander [30]	467	298	0.17	**3.1 ± 0.3**		–	>26 [220][c], >3 [300]
Stickel et al. [31]	1013	300	0.01	**>3.1 ± 0.6**[b]		–	–
Lazlo et al. [32]	270	295	0.3	2.8 ± 0.5, **3.3 ± 0.6**[d]		–	–
Harwood et al. [33]	>400	203–373	0.14	**3.6 ± 0.5**		–	–
Atkinson et al. [48]	40	295	0.0013	7.3 ± 0.5 [445.04, vac]	–	–	–
			0.3	–	2.6 ± 0.8[e], 3.1 ± 1.0[f]		
Bloss et al. [34]	1013		1.13	1.9 ± 0.2	–	Low. lim: 0.87 ± 0.15, up. lim.: 1.29 ± 0.22	>2 [340][c]
		295	0.12	–	3.0 ± 0.3, **3.3 ± 0.3**[g]	Low. lim: **0.99 ± 0.17**, up. lim.: **1.5 ± 0.3**	
This work	10–400	298	0.12	**3.5 ± 0.3**		**1.3 ± 0.3**	>(1.0 ± 0.2)[h] [340]

With 'Z' we refer to the absorption overlapped to IO in the spectral range between 320 and 440 nm (see Figs. 3 and 4). The original values of the references are given together with a homogenized reference at a selected resolution (if the original is lower than 0.4 nm) and vacuum wavelength. Bold case values refer to the homogenized reference (in some cases some additional corrections have been considered) used to calculate a recommended value.

[a] Corrections calculated assuming 426.95 nm, only orientative.
[b] Most likely systematic underestimation as a result of overestimation of ground state IO.
[c] Obtained by assuming $Z = I_2O_2$ and 100% yield from the IO self-reaction.
[d] After correction of σ_{I2} (21%).
[e] Convoluted and binned to 1.3 nm FWHM, transferred to $(4 \leftarrow 0)$ by relative scaling and MIntAS correction to 0.12 nm.
[f] After correction of σ_{I2} (21%).
[g] 10% upwards correction based on estimation of [33] in the same system.
[h] Originally determined at 356 nm and scaled to 340 nm to compare; independent of assignment, cross section per iodine atom.

vation of I amount is used, implying that

$$[\mathrm{I}]_0 = 2\,|\Delta[\mathrm{I}_2]| = 2\frac{\left|\Delta a_{\mathrm{I}_2}(\lambda_1)\right|}{L\sigma_{\mathrm{I}_2}(\lambda_1)} = [\mathrm{IO}]_{\max} = \frac{a_{\mathrm{IO}_{\max}}(\lambda_0)}{L\sigma_{\mathrm{IO}}(\lambda_0)}$$

$$\Rightarrow \sigma_{\mathrm{IO}}(\lambda_0) = \frac{\sigma_{I_2}(\lambda_1)a_{\mathrm{IO}_{\max}}(\lambda_0)}{2\left|\Delta a_{\mathrm{I}_2}(\lambda_1)\right|} \quad \text{(ii)}$$

where Eq. (i) was used to express concentration as a function of σ. $\Delta[\mathrm{I}_2]$ and $\Delta a_{\mathrm{I}_2}(\lambda_1)$ refer, respectively to the changes in concentration and OD of I_2 as a result of its rapid reaction with $\mathrm{O}(^3\mathrm{P})$, and $a_{\mathrm{IO}_{\max}}(\lambda_0)$ to the peak OD resulting from IO observed immediately after the reaction is initiated. The wavelengths λ_0 and λ_1 are arbitrarily selected. Typically, $\lambda_0 = 427.2$ nm ($4 \leftarrow 0$ transition) and $\lambda_1 = 500$ nm. The absorption cross section of I_2 at 500 nm is well known (Tellinghuisen [35], Saiz-López et al. [36], Spietz et al. [37]). The work of Lazlo et al. [32] is based on this approach, but provides a correction for I_2 photolysis at 193 nm. Harwood et al. [33] also used this method in one of their three independent determinations of $\sigma_{\mathrm{IO}}(4 \leftarrow 0)$.

Most previous approaches rely on applying conservation of oxygen atoms to reaction (4) or (5)

$$\Phi[\mathrm{O}]_0 = \Phi[\mathrm{O}_3] = \frac{\Phi a_{\mathrm{O}_3}(\lambda_2)}{L\sigma_{\mathrm{O}_3}(\lambda_2)} = [\mathrm{IO}]_{\max} = \frac{a_{\mathrm{IO}_{\max}}(\lambda_0)}{L\sigma_{\mathrm{IO}}(\lambda_0)}$$

$$\Rightarrow \sigma_{\mathrm{IO}}(\lambda_0) = \frac{\sigma_{\mathrm{O}_3}(\lambda_2)a_{\mathrm{IO}_{\max}}(\lambda_0)}{\Phi a_{\mathrm{O}_3}(\lambda_2)} \quad \text{(iii)}$$

where the factor Φ is the branching ratio of the first channel of reaction (5) and has a value of unity in reaction (4). The concentration of O atoms was determined in a separate experiment by substituting the precursor containing I atoms by O_2, and equating [O] to the final concentration of O_3 formed by recombination [30,33,34]. In general the chemical conditions must be adjusted to obtain an almost instantaneous and stoichiometric conversion of iodine or oxygen atoms into IO.

There are several sources of uncertainty in this way of determining σ_{IO}, concerning the underestimation of different reaction channels and overlapping of absorbers. Similarly the dependence on parameters such as Φ, or the necessity to undertake separate experiments to determine the concentration of oxygen atoms, are further potential sources of bias.

Finally, other authors have used the kinetic behaviour of IO to derive its absorption cross section. Harwood et al. [33] simulated a chemical reaction scheme including reactions (1), (2) and $\mathrm{IO} + \mathrm{O}(^3\mathrm{P}) \rightarrow \mathrm{I} + \mathrm{O}_2$. The σ_{IO} and the rate coefficient of reaction (2) were optimized to fit the observed decay of IO. Stickel et al. [31] used both reactions (1) and (4) as IO sources and as a consequence up to six different rate equations were numerically integrated to account for all production and loss processes. In this approach reference values of rate coefficients are required, and the knowledge of their accuracy is a source of uncertainty.

In the two studies of Cox et al. [28,29] a somewhat different technique was used to determine $\sigma_{\mathrm{IO}}(4 \leftarrow 0)$ and k_2. Molecular modulation was employed in a system based on reaction (1) [28] and (4) [29]. Simple kinetic modelling of the steady state photolysis cycle and the post-photolysis cycle is described by two equations having two unknowns, $\sigma_{\mathrm{IO}}(4 \leftarrow 0)$ and k_2, enabling the latter to be determined.

1.2. Knowledge about vibrationally excited IO

Previous studies have shown that reactions (1), (4) and (5) do not proceed completely to the formation of ground state $\mathrm{IO}(\mathrm{X}^2\Pi_{3/2}, v'' = 0)$. For example, Clyne and Cruse [38] stated that about a third of the IO generated in reaction (1) is vibrationally excited $\mathrm{IO}(\mathrm{X}^2\Pi_{3/2}, v'' = 1)$ (from here on denoted as IO^*)

$$\mathrm{I} + \mathrm{O}_3 \rightarrow \mathrm{IO}(\mathrm{X}^2\Pi_{3/2}, v'' = 0) + \mathrm{O}_2 \quad \text{(1a)}$$

$$\mathrm{I} + \mathrm{O}_3 \rightarrow \mathrm{IO}(\mathrm{X}^2\Pi_{3/2}, v'' > 0) + \mathrm{O}_2 \quad \text{(1b)}$$

Durie et al. [26] reported the formation of IO^* during the flash photolysis of mixtures of iodine vapour and O_2 at room temperature (most likely from reaction (4)), and Harwood et al. [33] observed IO^* as well from reaction (5). Gómez Martín et al. [39] have recently reported the observation of $\mathrm{IO}(\mathrm{X}^2\Pi_{3/2}, v'' = 2, \ldots, 6)$ (from here on denoted as IO^{**}) in absorption measurements by separation from overlapping I_2 and OIO spectral features in molecular time resolved absorption spectroscopy datasets obtained with a CCD camera.

Electronic ground state-vibrationally excited IO is rapidly quenched to the ground state. Using the data recorded in the course of this work, an estimated rate coefficient of $(1.9 \pm 0.4) \times 10^{-15}\ \mathrm{cm^3\ molecule^{-1}\ s^{-1}}$ for the quenching of vibrationally excited IO has been determined. Only at very low pressures (less than 100 mbar) the quenching proceeds slowly enough to observe a non-equilibrium population of vibrationally exited states of $\mathrm{IO}(^2\Pi_{3/2})$ on the time scale of milliseconds. This implies that $\mathrm{IO}(\mathrm{X}^2\Pi_{3/2}, v'' > 0)$ is most likely an additional source of bias in some determinations of $\sigma_{\mathrm{IO}}(4 \leftarrow 0)$ (e.g. [29,31]). On the other hand, although the spectrum of IO^* has been observed and assigned quite early [26,27], the estimate of $\sigma_{\mathrm{IO}^*}(\lambda)$ was up to now scaled effectively to the ground state $\sigma_{\mathrm{IO}}(\lambda)$ [31–34].

1.3. OIO absorption cross sections

The first observation of $\mathrm{OIO}(^2\mathrm{B}_1)$ was reported in 1996 by Himmelmann et al. [4], who produced it by flash photolysis of I_2 in the presence of O_3. One lower limit [19] and one determination of $\sigma_{\mathrm{OIO}(0,5,1 \leftarrow 0,0,0)}(\lambda)$ [18] can be found in the literature. Rowley et al. [18] constrained the branching ratio of OIO production in the reaction IO + BrO. By integrating both differential equations governing the time behaviour of [OIO] in the systems IO + IO and IO + BrO, in which reactions responsible for OIO removal were neglected, and by solving the resulting system of linear equations, they were able to constrain the branching ratio of OIO production in the reaction IO + IO and thereby determine the cross section of OIO.

1.4. Knowledge about end products of the $I_2 + O_3 + h\nu$ reaction system

Following the photolysis of mixtures of I_2 and O_3, it is well known that under some circumstances aerosols are produced. The aerosol produced in this study has been collected and analysed. It was shown to contain a complex higher oxide having the stoichiometry I_2O_5 [40]. This assignment is based on FTIR spectroscopy and in its high hygroscopicity, crystal shape and white colour. Clearly to generate a cluster of this composition, further iodine oxides other than IO and OIO must be formed in the gas phase following the IO self-reaction.

Other studies have reported the formation of broad band UV absorbers, attributed to aerosol ([28]) and/or gas phase species ([30,34,40]). It is tempting to attribute these absorption(s) to I_2O_2, which is likely to be a product of the IO self-reaction. Bloss et al. [34] were able to obtain an OD versus time formation curve, which seems to follow, at least partially, second order kinetics related to IO. Having determined the maximum branching ratio of I_2O_2 production in the IO self-reaction, they were able to derive a lower limit for its absorption cross section.

In the present study, not only one, but up to three broad band absorbers have been observed in the UV. Therefore it is necessary to reconsider the previous identification. A lower limit for the cross sections of one of these absorbers and estimations for the other two have been also derived in this work. The absorbers are denoted as 'X', 'Y' and 'Z' and their assignment is discussed below.

1.5. Objectives

The objective of the present manuscript is to describe the determination of an accurate and self consistent set of σs at relevant single wavelengths of the main absorbers involved in the I–O_3 photochemistry: IO, IO^*, IO^{**}, OIO and higher iodine oxides. The intention is to reduce uncertainties related to the overlapping spectra/ODs, to gain independence from kinetic hypothesis, used to determine concentrations, and to determine from each experiment *all* the σs of the species observed, in such a way that they are mutually consistent. In the accompanying paper [41] the σs of the species observed have been determined not only at single wavelengths but rather over the spectral region measured. As a result of the approach used in this work the complex kinetics of the system under study are not needed. Based on the cross sections determined here they will be discussed in a separate publication.

2. Experimental

2.1. Generation of radicals at known conditions

The reaction vessel (see Fig. 1) comprises a 120 cm-long double-jacketed quartz tube, which is temperature stabilized by a flow of pressurized air at ambient temperature 298 K. The optical windows at the entrance and exit of the vessel are made from quartz and are double walled and evacuated.

The photolysis flash system contains two Xenon flash tubes. Optical filters between the tube and the vessel are used to limit the wavelength of the photolysing radiation in the UV. Specifically this was used to minimize the photolysis of O_3 in its Hartley and Huggins bands forming $O(^1D)$.

Measurements are performed in flow mode. A stable flow of I_2 in N_2 is produced by passing a flow of N_2 through a thermostated and pressure stabilised glass vessel ($T = 273$ K) containing I_2. This flow can be diluted by an additional flow of pure N_2. O_3 is produced by passing a stream of O_2 through a silent discharge. The flows are controlled using calibrated mass flow controllers. Calibrated capacitance barometers measure the pressure in the vessel.

The broad spectrum flash (UV–vis) produced with Xenon tubes is able to photolyse I_2 and O_3. Thus, I and O atoms are

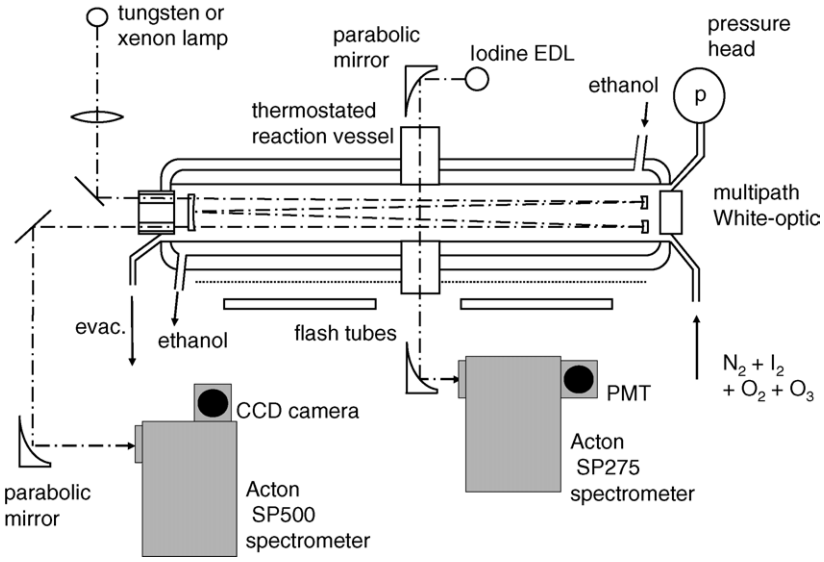

Fig. 1. Flash photolysis experimental set-up. It is conceived to perform synchronized multichannel time resolved absorption spectroscopy (white optics, CCD) and atomic resonance absorption spectroscopy.

formed

$$I_2 \xrightarrow{h\nu} \alpha I(^2P_{3/2}) + \beta I(^2P_{1/2}) \quad (6)$$

$$O_3 \xrightarrow{h\nu} O_2 + \delta O(^3P) + \varepsilon O(^1D) \quad (7)$$

Iodine atoms produced in the excited metastable state are rapidly quenched by collision with molecular oxygen

$$I(^2P_{1/2}) + O_2 \leftrightarrow I(^2P_{3/2}) + O_2(^1\Delta) \quad (8)$$

This quenching takes less than 0.8 μs at 10 mbar, which is the lowest pressure considered in this work. Such quenching is very effective due to resonance between energy levels of $I(^2P_{1/2})$ and O_2 (Young et al. [42]). The $O(^1D)$ excited oxygen atoms are also collisionally quenched in an excess of N_2 (Shi et al. [43]) and are deactivated in less than 0.4 μs at 10 mbar. The best time resolution of the detection system used in this work is 20 μs, implying that both $I(^2P_{1/2})$ and $O(^1D)$ are quenched prior to our observations.

Reactions (1) and (4) both produce IO. The latter reaction releases additional iodine atoms to react with O_3. Thus, two different sources of IO are simultaneously present in the experiments. In order to simplify the chemical system the second IO source was minimized using a glass filter able to block O_3 photolysis below 320 nm. Some photolysis of O_3 in its Chappuis band still occurs, producing mainly $O(^3P)$. As I_2 is in excess over oxygen atoms, the latter are quickly consumed (less than 1 ms after the flash for the lowest concentration of I_2 considered in this work).

During and following the formation of IO a number of further reactions take place. These include the self-reaction of IO. The time scale in which the chemistry under study takes place (≤40 ms) is short with respect to the vessel's purging time (∼3 s). This enables the assumption of a static mixture to be made for analysis purposes. The vessel is purged up to three times before each flash in order to remove secondary products, which could interfere in the reaction.

2.2. Detection

The experimental set-up (Fig. 1) is designed to simultaneously monitor all relevant molecular and atomic species. Molecular absorption is measured along the longitudinal axis of the reaction vessel (White-type multipath optic system, path length = 2430.5 cm). Atomic resonance absorption spectroscopy is performed along a short path cross axis (5.5 cm), in order to compensate for the significantly larger absorption cross section of I atoms, compared to the molecular absorption cross sections.

2.2.1. Multichannel time resolved molecular absorption spectroscopy (MTRAS)

A 150 W superquiet Xenon arc lamp is used as absorption light source. After having traversed the vessel, the analysis light is focused onto the entrance slit of a Czerny–Turner spectrometer (500 mm focal length). A CCD camera (Roper Scientific) equipped with a 1024 × 1024 silicon detector chip (SiTE) is employed as detection device (pixel size 26 μm × 26 μm).

The CCD can be operated either *statically* recording individual spectra at pre-set times or *time resolved* recording sequences of full spectra at set time intervals. For the time resolved mode the chip of the CCD is masked by a horizontal slit such that roughly five rows are exposed. By shifting all rows step wise from the exposed area down under the mask, time resolved recording of spectra is achieved. The fastest shifting time is 20 μs. By this mechanism each spectrum is exposed during five shift intervals and accumulates the temporal variation of signal during this time. This corresponds to a 5-point "moving-average" smoothing of the original temporal behaviour of optical density versus time. The shape of the smoothing kernel function is not rectangular, but determined by the characteristic illumination function on the chip of the CCD. Without correction, the effective resolution in time is therefore limited to roughly 100 μs. This is sufficient, if the observed structures change slowly in comparison to this effective temporal resolution. If faster processes had to be monitored, then a deconvolution in time would improve the effective temporal resolution slightly using a *measured* characteristic function of illumination. In the present work, however, all processes of interest were kept sufficiently slow to enable the direct usage of time resolved signals without deconvolution.

In the majority of kinetic experiments, a low spectral resolution (FWHM = 1.3 nm) was selected by using a combination of an entrance slit width of 100 μm and a grating having 150 grooves/mm (linear dispersion 0.32 nm pixel^{-1}). This enables a spectral window containing the absorptions of all the relevant reactant and product molecular species involved in the reaction from roughly 300 to 600 nm to be measured in a single recording, without changing the grating's position. The reactants I_2 and O_3 were measured using their well known strong absorption features in the visible around 500 nm [35–37] and in the UV around 260 nm (see Bogumil et al. [44] and references therein), respectively.

By using the CCD in time resolved mode and synchronous photolysis of the mixtures of I_2 and O_3 in the bath gases N_2 and O_2, the simultaneous measurement of the concentration dependent molecular absorptions results. A two-dimensional raw image consisting of intensities plotted on a grid of time steps versus detector pixels is obtained. Wavelength calibration is achieved by measuring the calibration spectra of a Hg–Cd line source in static mode. In this manner the two-dimensional grid of data has the dimensions of time versus wavelength.

Dark current and detector characteristics are measured using exactly the same procedure as in the recording of the absorption dataset, but with the shutter in front of the spectrometer closed. By subtraction of this background signal from the measured intensities the effects of the detector characteristics and the dark current are corrected, yielding a data set of intensities $I(\lambda, t)$. The reference spectrum, $I_0(\lambda, t)$, is obtained with the same procedure, but flashing mixtures of only N_2 and O_2. Any optical deformation within the vessel, by the mirror mounts, or the optical windows are thus identical in $I(\lambda, t)$ and $I_0(\lambda, t)$. This procedure also results in the removal of the majority of the scattered light coming from the flash and interfering with the

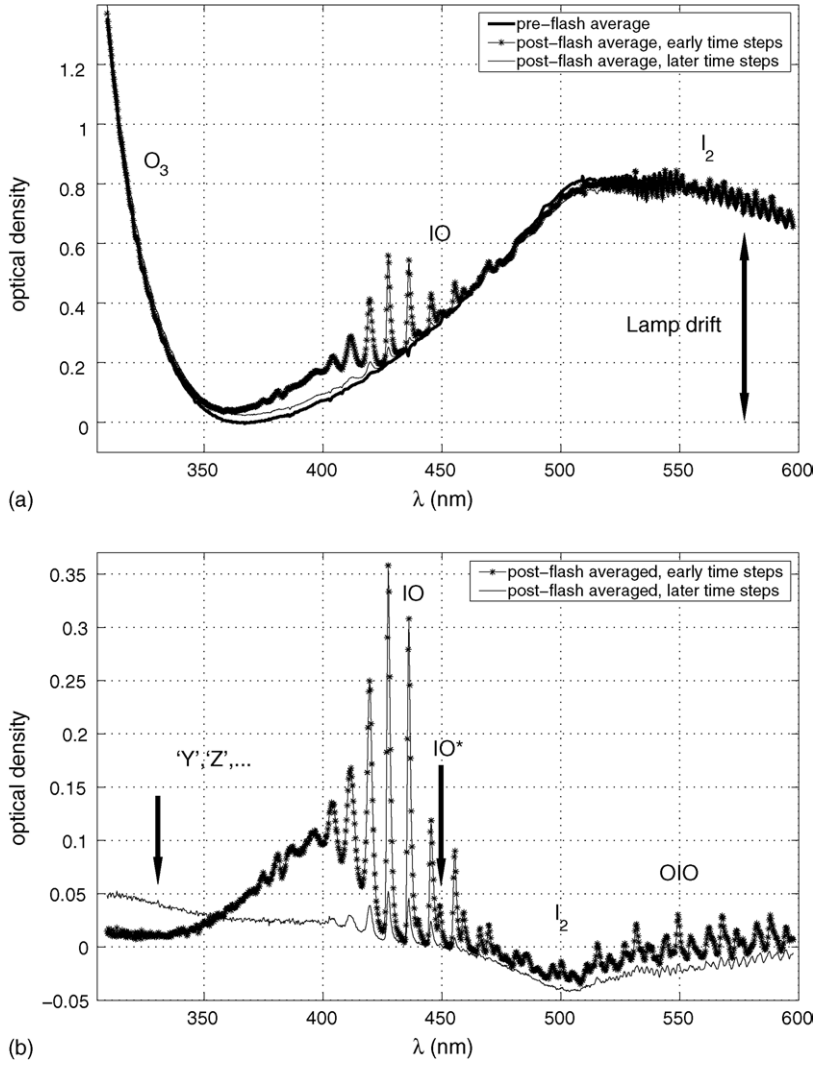

Fig. 2. Lamp drift correction of the kinetic datasets: pre-flash averaged spectral profile is subtracted from each spectral profile of the data recording. In (a) the pre-flash spectrum and two spectra at different time steps are shown. After correction (b), spectral features corresponding to different species can be better recognized. 'Y' and 'Z' refer to broad band UV absorbers, most likely higher iodine oxides.

analysis light. The OD is then obtained via the equation

$$a(\lambda, t) = \ln\left(\frac{I_0(\lambda, t)}{I(\lambda, t)}\right) \quad \text{(iv)}$$

A set of time-averaged OD spectral profiles corresponding to a single dataset and derived as explained above are shown in Fig. 2.

2.2.2. Atomic resonance absorption spectroscopy

An electrodeless discharge iodine lamp is used as light source for resonance absorption spectroscopy. After having traversed the reaction vessel through the cross axis the analysis light is focused onto the entrance slit of a Czerny–Turner spectrometer (250 mm focal length), operated with a 1200 grooves/mm holographic grating. With this grating it is possible to resolve the I($^2P_{3/2}$) 183.038 nm resonance transition from neighbouring lines, with the PMT as detector. The atomic resonance absorption was previously calibrated with the molecular absorption set-up in I_2/O_2 photolysis experiments by monitoring the I_2 photolysis at 500 nm.

In the experiments conducted for this work the atomic resonance and the molecular absorption set-ups are synchronized and therefore simultaneous recordings of atomic I and molecular species can be obtained. Further details in the experimental set-up and the determination of the oscillator strength of the I($^2P_{3/2}$) 183.038 nm resonance transition can be found in Spietz et al. [45].

3. Theory

3.1. Approach: conservation of iodine

The concept of iodine conservation within the chemical system, as applied in this work to the determination of σs, equates the initial concentration of I atoms (contained in the initial I_2) to the concentration of I atoms, present in molecules or as atoms,

after the flash *at each time step* of the reaction. It assumes that all absorbing iodine containing species of significant concentrations are measured and that the amount of any non-absorbing I containing species is known or negligible. Note that in previous determinations based on conservation of iodine (or oxygen), this was applied to a *single time step* corresponding to the peak IO concentration (Eq. (ii) or (iii)). In contrast, in our approach, N linear equations as function of the time step for reaction, t_i, are considered

$$2[I_2]_0 = 2[I_2](t_i) + [I](t_i) + [IO](t_i) + [IO^*](t_i) + [IO^{**}](t_i) + [OIO](t_i) + [X](t_i) + [Y](t_i) + [Z](t_i) + \cdots \quad (v)$$

The concentration of each absorber 'M' (see Eq. (i)) is given by the Beer–Lambert law

$$[M](t_i) = \frac{a_M(\lambda, t_i)}{L\,\sigma_M(\lambda)} \quad (vi)$$

Note that the wavelength λ_M of the transient OD (a_M) in the above formula corresponds to that wavelength used for the determination of the σ of the absorber M (M = IO, IO^*, IO^{**}, OIO, X...). If Eq. (vi) is substituted in Eq. (v), these N equations can be arranged in the following way

$$\{2([I_2]_0 - [I_2](t_i)) - [I](t_i)\}L = \frac{a_{IO}(\lambda_{IO}, t_i)}{\sigma_{IO}(\lambda_{IO})} + \frac{a_{IO^*}(\lambda_{IO^*}, t_i)}{\sigma_{IO^*}(\lambda_{IO^*})} + \frac{a_{IO^{**}}(\lambda_{IO^{**}}, t_i)}{\sigma_{IO^{**}}(\lambda_{IO^{**}})} + \frac{a_{OIO}(\lambda_{OIO}, t_i)}{\sigma_{OIO}(\lambda_{OIO})} + \frac{a_X(\lambda_X, t_i)}{\sigma_X(\lambda_X)} + \frac{a_Y(\lambda_Y, t_i)}{\sigma_Y(\lambda_Y)} + \frac{a_Z(\lambda_Z, t_i)}{\sigma_Z(\lambda_Z)} + \varepsilon(t_i) \quad (vii)$$

where $\varepsilon(t_i)$ represents the error in predicting the observations in the left hand side with the proposed model. Multiple linear regression (MLR) is used to determine the σs (Section 3.2). Note that separated and instrument independent optical densities a_M are required (Section 3.3).

The important advantages of this approach are its independence of mechanistic hypotheses and kinetic reference data. The only reference data required is the absorption cross section of I_2 and the oscillator strength of $I(^2P_{3/2})$. The former has been checked (see Spietz et al. [37]) and its uncertainty could even be further reduced by our determination. The latter was also determined and inhomogeneities were accounted for by additional empirical calibration. A second advantage is that the approach enables *simultaneous* and *consistent* determination of cross sections of all different species observed in the experiment. This is an important improvement with respect to most previous studies, which had to determine selected cross sections under idealized conditions ignoring others, thus being forced to approximate other cross sections iteratively. Errors in the reference data and in the determination of the first cross section within the iterative chain propagate into the last estimates producing increasing uncertainties for the results determined at the end of the chain. Also such approaches usually had to rely on kinetic reference data. Therefore the resulting estimated cross sections are not independent estimates. A third advantage is the increased coverage in time. Within the iterative approaches always only a limited time window of data containing either the earliest products – usually the more or less instantaneous production of IO and OIO – or only the decay of an absorber can be used. Full temporal coverage usually has to be avoided because of the content of other products or their kinetics have to be modelled with multi-parameter kinetic mechanisms. In the present approach the number of unknowns is limited to the absorption cross sections while the later products of reaction are included. Thus it is possible to use also observations from later times within the course of reaction, being the quality of the results obtained improved by an increased averaging effect.

Note that the cross sections resulting from the method of iodine conservation are cross sections per iodine atom. Once the stoichiometry of the molecule is identified by kinetic or spectroscopic considerations, their absorption cross sections can be converted to cross sections per molecule.

3.2. Separation of overlapping spectra

Eq. (i) can be also written for a multi-component system with n different absorbers as follows:

$$I(\lambda, t) = I_0(\lambda, t)\,\exp\left(-L\sum_{k=1}^{n} c_k(t)\sigma_k(\lambda)\right) \Leftrightarrow$$

$$a(\lambda, t) = L\sum_{k=1}^{n} c_k(t)\sigma_k(\lambda) \quad (viii)$$

The OD measured at a given wavelength and time $a(\lambda, t)$ is a mixture of the ODs corresponding to the different species present in the mixture at that time and absorbing in the same wavelength range. In our case, OD data arrays obtained by applying Eq. (iv) to CCD data contain at least eight different overlapping absorbers, including both reactants and products.

Let us assume that the column densities at any time of all species are known, and that the absorption cross sections are not known. The following matrix equation describes in such case the multivariate linear model (viii) for all wavelengths and time steps

$$\boldsymbol{Y} = \boldsymbol{C}\boldsymbol{S} + \boldsymbol{E} \quad (ix)$$

The matrix $\boldsymbol{Y}$ – matrix of observations – contains on each column the transient OD at a given wavelength. The columns in matrix $\boldsymbol{C}$ – the so called mixing matrix or matrix or coefficients – are the transient 'column densities' of each absorber contained in the mixture. Finally, the rows of $\boldsymbol{S}$ – unknowns – are the spectral absorption cross sections of each absorber. $\boldsymbol{E}$ is a matrix of prediction error. The matrix representation of the Beer–Lambert law for a multicomponent system is a standard in the so called 'chemometrics'. More details can be found e.g. in Brown et al. [46].

If the absorbers have different temporal behaviours, (a condition, which can be mathematically expressed as linear independence of the columns in the matrix $\boldsymbol{C}$), it is possible to separate the observed data into several linear components – one for each absorber – using multivariate analysis techniques based on the inversion of the mixing matrix, for example principal components analysis (PCA) or, independent components analysis (ICA) (Gómez Martín et al. [39] and references therein). It is also possible and sometimes even necessary to use multivariate multiple linear regression (MMLR) if reference spectra are available. Finally, it is possible to combine MMLR with the previously mentioned techniques.

The success of these techniques depends on the spectral range of application. For the absorbers IO^{**}, OIO and I_2, a combination of PCA, ICA and MLMR was used to achieve their separation. For IO and the broad band UV absorbers, identified in this work, iterative spectral MMLR was applied. Thus for each dataset it is possible to retrieve sets of well separated OD temporal behaviours (a_M) at the wavelengths selected for use in the set of Eq. (vii).

3.3. Resolution and binning correction

It is well known that a low instrument resolution broadens σs measured at higher spectral resolution. In addition, binning on the CCD pixels also affects the observed absorption cross section. In order to compare the results presented in this work to published cross sections and to review critically those previous results the effect of resolution and undersampling on the cross sections was studied (Spietz et al. [47]). For $\sigma_{IO}(4 \leftarrow 0)$ a clear dependence of the measured σ and the wavelength of the peak absorption on the spectral resolution could be shown. An analytical relationship between $\sigma_{IO}(\lambda)$ obtained for low resolution/coarse binning and those obtained for high resolution/fine binning measurements has been deduced. Using this relationship, a method to obtain the best approximation to the real peak OD of a vibronic-rotational absorption band from low resolved and coarsely binned measurements has been developed and applied to the IO case. This method is called multichannel integrated absorption spectroscopy (MIntAS). It can be understood as an "inverse convolution" of low resolved and coarsely binned intensity spectra, which does not require knowledge of the instrumental line shape, but a high resolution relative reference spectrum. This spectrum has been measured with the same set-up by using a 1200 grooves/mm grating and 75 μm slit width (FWHM = 0.12 nm), which yields a line shape of the $(4 \leftarrow 0)$ band determined by the molecule and not any more by the instrument function.

3.4. Determination of absorption cross sections by multiple linear regression

Once our OD temporal behaviours are separated and corrected for non-linear instrumental effects, the iodine conservation model can be applied. The set of Eq. (vii) can be also written in matrix form

$$\boldsymbol{y} = \boldsymbol{A}\boldsymbol{x} + \boldsymbol{\varepsilon} \quad \text{(x)}$$

where $\boldsymbol{y} = (\{2([I_2]_0 - [I_2](t_i)) - [I](t_i)\}L)$, $i = 1, \ldots, N$, is the observational vector (with column density units). $\boldsymbol{A} = (\boldsymbol{a}_{IO}, \boldsymbol{a}_{IO^*}, \boldsymbol{a}_{IO^{**}}, \boldsymbol{a}_{OIO}, \boldsymbol{a}_X, \boldsymbol{a}_Y, \boldsymbol{a}_Z)$ is the matrix of coefficients. Each column of $\boldsymbol{A}$ contains the OD temporal behaviour of one absorber. Therefore, $\boldsymbol{a}_M$ is a vector with components $\boldsymbol{a}_M(\lambda, t_i)$, $i = 1, \ldots, N$. The vector of unknowns is $\boldsymbol{x} = (1/\sigma_{IO}(\lambda_{IO}), 1/\sigma_{IO^*}(\lambda_{IO^*}), 1/\sigma_{IO^{**}}(\lambda_{IO^{**}}), 1/\sigma_{OIO}(\lambda_{OIO}), 1/\sigma_X(\lambda_X), 1/\sigma_Y(\lambda_Y), 1/\sigma_Z(\lambda_Z)\ldots)^T$. Finally, $\boldsymbol{\varepsilon}$ is a vector of prediction error. The number of unknowns is equal to the number of absorbers included (here up to seven depending on the dataset), and the number of observations is equal to the number of reasonable time steps (which depending on the existence of other unaccounted absorbers can reach up to 500). This is therefore an overdetermined system of linear equations.

Assuming a Gaussian distribution of the residuals and linear independence of the variables $\boldsymbol{a}_M$, the components of the vector $\boldsymbol{x}$ can be estimated by using the MLR technique.[1] The optimal solution is given by

$$\boldsymbol{x} = (\boldsymbol{A}^T\boldsymbol{A})^{-1}\boldsymbol{A}^T\boldsymbol{y} \quad \text{(xi)}$$

Determining $\boldsymbol{x}$ for different total reaction times enables the consistency of the assumptions about the number of absorbing species present. The number of equations or time steps included in the least squares fitting is determined iteratively and selected such that the residual is distributed normally. The stability of the solution is established calculating the parameters for successively increasing fitting time intervals. The dependence of the parameters on the fitting interval length is then assessed. If systematic deviations are found, this implies that unaccounted absorbers are present in the mixture. For the determination of σs, it is an inherent assumption that columns in $\boldsymbol{A}$ are independent (i.e. the normal matrix $\boldsymbol{A}^T\boldsymbol{A}$ is invertible). Thus the approach is limited by any multicollinearity (linear dependence between the assumed independent variables $\boldsymbol{a}_M$).

4. Results

4.1. Datasets

Table 2 contains a description of the kinetic experiments at different conditions used in this study. Experiments typically comprise 100 single flash times in order to obtain a good signal to noise ratio. Initial conditions have been varied to check for the independence of the results obtained.

The pre-processing of the experimental data includes the elimination of spurious changes in OD caused by light source drift between $I(\lambda, t)$ and $I_0(\lambda, t)$ measurements (see Fig. 2). As no significant drift occurs within a single measurement (∼20 ms) long term drift effects are corrected by subtracting from each dataset its own averaged pre-flash spectral profile. A further consequence is that I_2 and O_3 temporal behaviours become relative

[1] In MLR there is only one dependent (observed) vector variable. MMLR (Section 3.2) refers to a multiple linear regression where there are several observed variables (multivariate). Therefore, the observations are contained in a matrix, and a matrix of coefficients to be determined: $\boldsymbol{Y} = \boldsymbol{A}\boldsymbol{X} + \boldsymbol{E}$.

Table 2
Experimental conditions of kinetic datasets

Group	N_{exp}	P_{vessel} (mb)	$[N_2]^a \times 10^{18}$	$[O_2]^a \times 10^{18}$	$[O_3]_0^b \times 10^{15}$	$[I_2]_0^b \times 10^{13}$	$[I]_{max}^c \times 10^{13}$	$[IO]_{max}^d \times 10^{12}$
1	8	40–400	0.5–10	0.4–1	2	5.4	1	7.5–8
2	7	100–400	0	2–10	2	5.4	1	6.5–7
3	6	40–400	0.5–10	0.4–1	8.2	4.4	1	5
4	11	10–40	0	0.2–1	0.5–2	1–6	3–9	2–8
5	6	10–40	0.1–0.6	0.1–0.4	0.5–2	0.3–1	2–6	1.5–5.5
6	6	40	0	1	0.1	5.4	1	7

All concentrations are given in molecule cm^{-3}.
[a] N_2 and O_2 concentrations have been estimated from the total pressure in the vessel and the readout of the flow controllers. Uncertainty ~10%.
[b] I_2 and O_3 concentrations are obtained either by measuring pure I_2 and O_3 spectra in static mode previous to the kinetic series and/or by using optical densities recorded in kinetic mode after the photolysis flash. Error estimates (<15%) account for random noise of the detection device as well as for drifts of $[I_2]$ and $[O_3]$ along the experiment and lamp drifts.
[c] Calculated as indicated in Section 2.2.2. The uncertainties (<10%) are obtained as the standard error estimation of the least squares fits applied in the calibration of the set-up.
[d] Calculated using σ_{IO} determined in this work. The uncertainties (<10%) consider the uncertainty in σ_{IO}, as well as the estimated error of the time behaviour of IO.

to the initial concentrations. For O_3, the transient OD change resulting from reaction (1) is below the detection limit within the observed spectral window and therefore does not affect the determination of other UV absorbers. For I_2 the correction for lamp drift is advantageous, because the first term of Eq. (vii) describes the difference between the I_2 at a given reaction time t and its initial concentration: $[I_2]_0 - [I_2](t)$.

4.2. Separation of the temporal behaviour of spectrally overlapping ODs

4.2.1. Separation of the absorbers: IO, 'X', 'Y' and 'Z'

First we concentrate on a wavelength region between 340 nm (chosen to avoid complications due to further UV absorbers, see below) and 435 nm (chosen to avoid complications derived from IO^* and I_2). From a knowledge of the kinetic behaviour of the different chemical species and/or by applying DOAS, the differences between spectra obtained at different time steps are generated. These yield separated relative spectra of IO and 'Z'. A second broad band spectrum ('X') is retrieved by fitting a polynomial underneath the IO spectrum in a spectral profile averaged in a time interval of about 0.25 ms immediately after the flash. A MMLR is performed, accounting for the reference IO spectrum and the two spectra of 'X' and 'Z' as independent variables. Arbitrarily scaled temporal behaviours of the absorptions of IO, 'X' and 'Z' result. Results are shown in Fig. 3. The analysis can also be applied in such a way that the temporal behaviours obtained by MMLR, as indicated above, are used as independent variables in a further MMLR, in order to retrieve spectra. Provided that the fit is performed in the same spectral range, the retrieved spectra are in good agreement with the initial input.

It was observed that if the fitting spectral window is enlarged down to approximately 310 nm, some systematic features appear in the residuals (Fig. 4e), indicating the presence of a further UV absorber 'Y'. The OD time profiles averaged between 310 and 340 nm show a behaviour different to that of 'Z' (Fig. 3d). Similarly the temporal curves obtained disagree with those used as input.

The strong spectral overlap of 'Y' and 'Z' and the absence of vibrational features impede the use of the mathematical techniques explained above to separate them. The experimental approach used in this work is not suitable for an unambiguous identification of the higher iodine oxides (see Section 5.2.3), and as a result the conditions of the mathematical models used for optimal extraction of information are not fulfilled. To gain some knowledge about 'Y' from the data available it is necessary to skip temporarily the premise of being independent from kinetic hypothesis. One of the important products of the IO self-reaction is expected to be the IO-dimer, I_2O_2. Some broad band absorptions, similar to 'Z', have been previously assigned tentatively to I_2O_2 (see [34]). In our case, the temporal curve corresponding to 'Z' does not follow the expected second order formation (see Fig. 3d), even at the beginning of the curve, as argued in [34]. Even if different sinks are considered (dissociation, $I_2O_2 + I$, etc.) the temporal behaviour of the absorption 'Z' cannot be modelled by the kinetics of the IO-dimer. It can be concluded therefore that 'Z' is not I_2O_2. In contrast, the averaged time profile between 310 and 340 nm, containing the OD due to 'Y', (see Fig. 3d) does show a rate of formation having an apparent second order dependence on IO. From its temporal behaviour 'Y' is tentatively assigned to be I_2O_2. The 'Y' spectrum is fitted, by using the result of numerically integrating the branch differential equation corresponding to reaction (2c), that is

$$[I_2O_2](t) - [I_2O_2]_0 = k_{2c}[M] \int_0^t ([IO](t'))^2 \, dt' = \varphi \int_0^t (a_{IO}(t', \lambda_0))^2 dt' \quad \text{(xii)}$$

where $\varphi = k_{2c}[M]/(L\sigma_{IO}(\lambda_0))^2$ and $[I_2O_2]_0 \approx 0$. The constant φ is unknown, because whether the rate constant of reaction (2c) nor $\sigma_{IO}(\lambda_0)$ are known a priori. Nevertheless, the scaling of the time behaviour is unimportant in the separation procedure because the only objective is to obtain a pure optical density. Therefore, no assumption on the branching ratio is needed. By numerically integrating the squared absorption of IO at a given wavelength a normalized concentration is obtained (Fig. 4c),

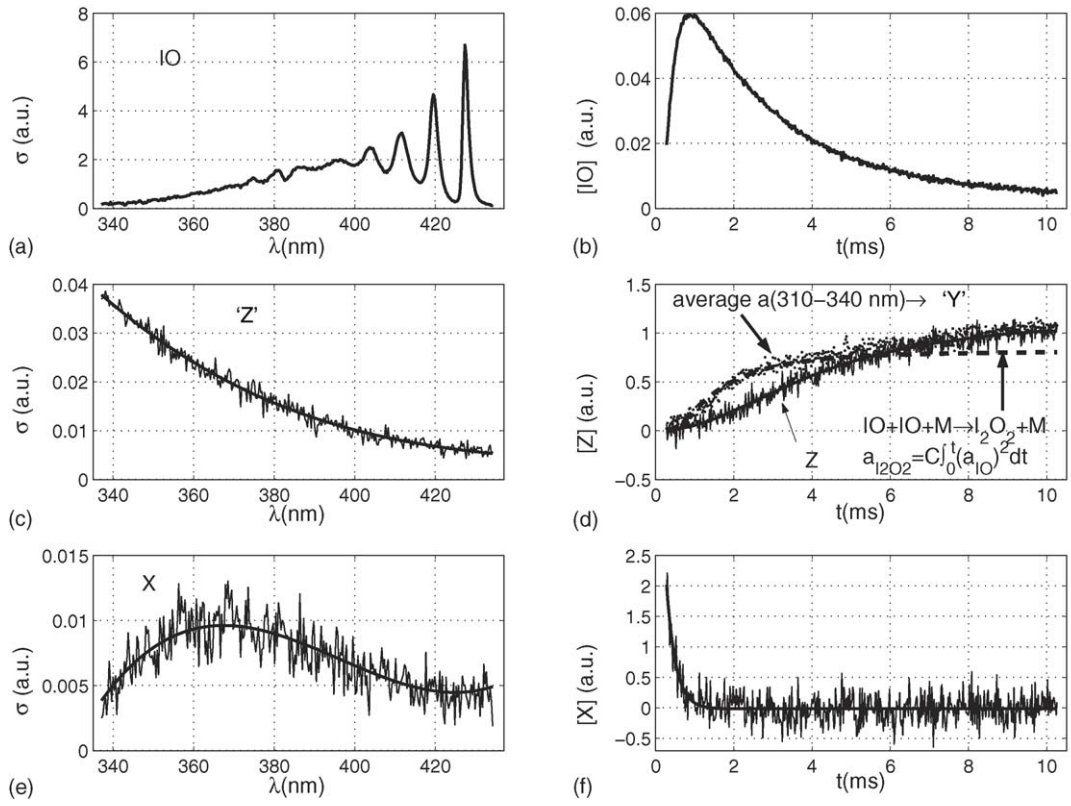

Fig. 3. Results of separation of overlapping spectra between 340 and 435 nm. Spectra of IO (a), 'Z' (c) and 'X' (d) are obtained by combination of different techniques. The measured OD in the spectral range 340–435 nm is regressed against them, and temporal behaviours are subsequently obtained (panels b, d, and f, respectively). Panel d shows the disagreement between the temporal behaviour of 'Z' and the modelled I_2O_2 concentration curve (dash line) obtained by using Eq. (xii). The kinetic assignation of I_2O_2 to a further absorber observed from 310 to 340 nm is more plausible.

and the corresponding spectrum obtained by MMLR (Fig. 4d) is automatically scaled such that the product of both quantities gives the true pure optical density.

The results obtained are shown in Fig. 4. The panels 4a and 4b show the time curves used as input in Eq. (ix), and the panels 4b and 4c the resulting spectra. Fig. 4e compares the residuals of the MMLR when 'Y' is and is not included on it, and demonstrates that the assignment of I_2O_2 to 'Y' is very plausible. From this point on we will refer to 'Y' as I_2O_2. The assignment of 'X' and 'Z' are discussed below.

The formation of a deposit, which is white but absorbing in the UV, on the mirrors and the windows of the vessel together with the strong absorption of O_3 reduce the transmission of the analysis light in the UV dramatically, such that after two or three experiments the signal below 320 nm reaching the detector has decreased significantly and the signal to noise becomes poor. Thus only selected experiments are suitable for the identification of the spectrum attributed to I_2O_2. It was therefore not possible to establish a systematic dependence of this absorption on pressure or on the mixing ratio of the precursors.

In Section 4.4, the solution of Eq. (ix) (the mass balance equation) is discussed. The temporal behaviours of OIO, and 'Z' and I_2O_2 are linearly dependent, particularly at longer reaction times when OIO is small. Thus when OIO, I_2O_2 and 'Z' are explicitly considered in the matrix $\boldsymbol{A}$ for all reaction times from 0.5 to 10 ms, then the three individual components cannot be separated. The solution to this analytical problem for determination of the σ_{OIO} is to solve the matrix $\boldsymbol{A}$ over time intervals where the OIO is large and to reduce the two absorbing adducts, I_2O_2 and 'Z', to one effective adduct by using *only* the measured time behaviour of 'Z'. This is consistent with the aim of being independent of kinetic hypothesis in the determination of σ_{IO}, σ_{IO^*}, $\sigma_{IO^{**}}$, σ_{OIO} and σ_Z, although it also raises the question of interpreting the cross section obtained for 'Z'. The consequences of this decision are discussed below.

4.2.2. Separation of the absorbers: IO^{**}, OIO and I_2

A combination of PCA, ICA and MLR is used to separate IO^{**}, OIO and I_2. This procedure is described in detail in Gomez Martin et al. [39] (note that in the reference IO($X^2\Pi_{3/2}$, $v'' > 0$) is collectively termed as IO^*). The curves of IO^{**} and OIO resulting from this analysis are shown in Fig. 5. The corresponding spectra can be found in [39] and in the accompanying paper. The temporal behaviour of OD for I_2 at 500 nm yields the concentration from knowledge of the absolute absorption cross section of I_2 at 500 nm. In this study a value of $\sigma_{I2}(500\,\text{nm}) = (2.191 \pm 0.020) \times 10^{-18}$ molecule/cm^3 (see [37] and references therein) has been used.

4.2.3. Separation of the absorber IO^*

Absorptions of 'Z' and I_2 are not negligible in the spectral range where IO^* is observed. Therefore, their contributions were subtracted from the total absorption and the resultant attributed to IO^* during the time interval where IO^* is present. An I_2 OD

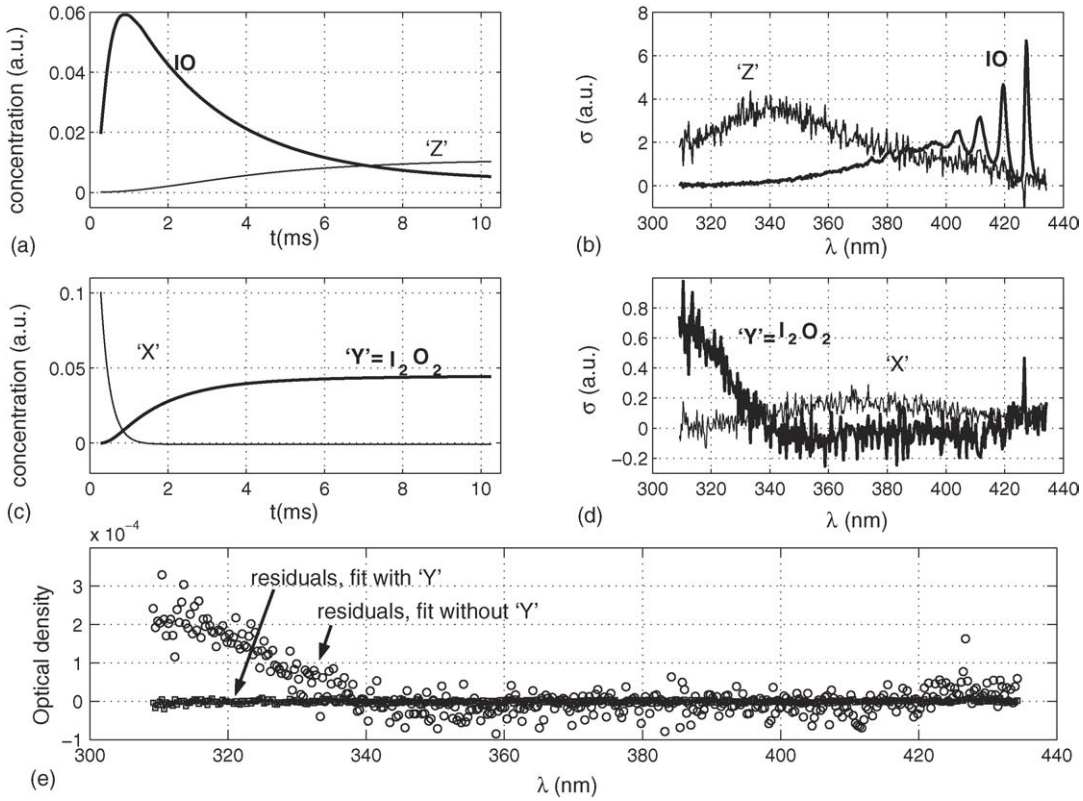

Fig. 4. Results of separation of overlapping spectra between 310 and 435 nm (panels b and d). OD between 310 and 435 nm is regressed against the temporal behaviours (panels a and b) of IO, 'X', 'Z' and the modelled temporal behaviour of I_2O_2. The spectrum of a further absorber is retrieved (panel d). In panel e residuals of the same regression fit with and without the modelled temporal behaviour of I_2O_2 are compared. Note that in the second case the residual contain a similar spectral feature to that retrieved in the first one. Kinetic assignation of this spectrum to I_2O_2 is therefore plausible.

is readily calculated by multiplying the I_2 temporal behaviour, obtained as explained in [39], with a reference I_2 spectrum, measured with the same experimental set-up in static conditions. Similarly, the OD attributed to 'Z' is reconstructed by multiplying its spectrum with its temporal behaviour, both obtained as explained in Section 4.2.1. When the spectral window for IO^* is free of I_2 and 'Z', the temporal behaviour of IO^* is obtained from the maximum OD at 449.3 nm ($3 \leftarrow 1$). Sepa-

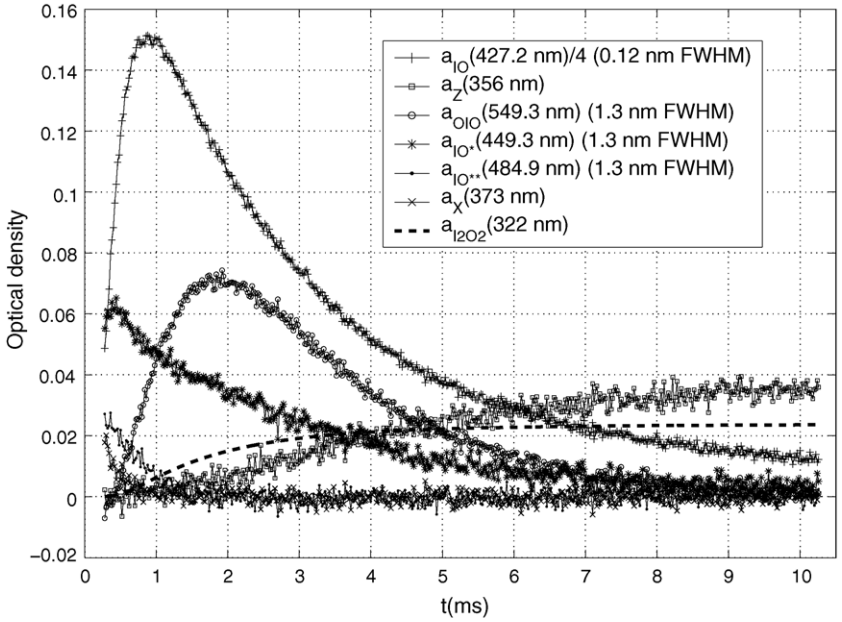

Fig. 5. OD temporal behaviours of the different species observed at the wavelengths selected for the determination of their absorption cross section. The I_2O_2 time behaviour was calculated by using Eq. (xii).

Table 3
Results of MIntAS

Species	FWHM		Correction/scaling	Non-linearity (%)
	Lo-res (nm)	Hi-res (nm)		
IO($4 \leftarrow 0$)	1.3	0.12	(Correction applied before I conservation) average scaling: 1.64 ± 0.04	5
$IO^*(1 \leftarrow 3)$	1.3	0.35	1.82 ± 0.21	1
$IO^{**}(1 \leftarrow 2)$	1.3	0.35	1.82 ± 0.21	1
OIO(0, 5, $1 \leftarrow 0$, 0, 0)	1.3	0.35	1.14 ± 0.05	0.1
IO($2 \leftarrow 0$)	1.3	CRDS	Validation: 11 ± 3 (MIntAS) 9.9 (conv. + bin.)	16

Previous to application of the iodine conservation (Eq. (x)), the influence of spectral resolution on the apparent optical density was characterized. The non-linearity in IO($4 \leftarrow 0$) was judged to be large enough to justify the application of MIntAS *before* iodine conservation. In all the other cases a simple scaling factor is applied *after* iodine conservation. The application of MIntAS to the ($2 \leftarrow 0$) band is a validation of the method. The uncertainties have been defined elsewhere [47].

rated temporal behaviours of all absorbers monitored are shown in Fig. 5.

4.3. Correction of resolution related experimental effects

The analysis technique MIntAS has been applied to absorptions of the bands IO($4 \leftarrow 0$), $IO^*(3 \leftarrow 1)$, $IO^{**}(1 \leftarrow 2)$ and OIO(0, 5, $1 \leftarrow 0$, 0, 0), which are used for the iodine mass balance (Eq. (vii)) cross section retrievals. Results are summarized in Table 3, where the average scaling factors between spectrally low and high resolved optical densities are shown. In general the instrumental resolution causes a small, significant and non-linear dependence of the apparent optical density on concentration. In the case of the IO($4 \leftarrow 0$) band, the deviation from Lambert–Beer law represents a change of about 5% with respect to the mean scaling factor.

As a result of the above, the IO time traces have been corrected for this instrumental resolution effect *before* being used in Eq. (xi). For $IO^*(3 \leftarrow 1)$ and $IO^{**}(1 \leftarrow 2)$ absorption bands, the non-linearity is less than 1% and for OIO is less than 0.1%. Therefore, the non-linear correction is assumed negligible and a constant correction factor is applied to the calculated cross sections *after* solving Eq. (x).

MIntAS has been also applied to the ($2 \leftarrow 0$) transition for validation purposes. The *instrument independent* value of σ_{IO} for the "band head" (band origin) of the ($2 \leftarrow 0$) transition at 445.04 nm was obtained by Atkinson et al. [48] by scaling their cavity ring-down (CRD) spectrum recorded at a resolution of 0.0013 nm FWHM with a low resolution reference cross section from Lazlo et al. [32]. This high resolution enables the rotational structure to be resolved. The scaling was achieved by convolving the CRD spectrum with the characteristic function of the monochromator of [32] and by using the *apparent* absorption cross section reported for the ($2 \leftarrow 0$) band in that work. Note that this band has been successfully studied by laser induced fluorescence (LIF) (Inoue et al. [49]), indicating that the $A(^2\Pi_{3/2}, v' = 2)$ state of IO is relatively long lived in comparison to the $A(^2\Pi_{3/2}, v' = 4)$ IO state, which is a strongly pre-dissociative state. As a consequence the ($4 \leftarrow 0$) band presents only a smooth band contour and can be adequately monitored with a spectral resolution of 0.12 nm FWHM. In contrast the ($2 \leftarrow 0$) band has strong rotational structure, which is not well resolved for the same resolution.

The scaling obtained by applying MIntAS to the ($2 \leftarrow 0$) band measured at 1.3 nm FWHM, using the CRD spectrum of [48] as reference, has been compared to the result of convolving and binning this CRD spectrum to obtain the spectral resolution of 1.3 nm FWHM used in this work. As shown in Table 3, both procedures yield very similar scaling factors between the low and the high resolved values. Moreover, by transferring the absolute scaling of the degraded CRD spectrum to the maximum of the ($4 \leftarrow 0$) band of our low resolved spectrum and by subsequently applying MIntAS with a target resolution of 0.3 nm FWHM, the retrieved value for the maximum of the ($4 \leftarrow 0$) band is in good agreement with the value of Lazlo et al. [32] (see Table 1). This validates our analytical approach.

4.4. Absolute absorption cross sections of iodine oxides

The σs of the absorbers considered in Eq. (vii) at the selected wavelengths have been retrieved by MLR. The results are shown in Table 4. The uncertainties in wavelength are given by the absolute maximum of the calibration residual. The error estimates of the absorption cross sections are given by one standard deviation of the set of results obtained from 44 datasets analysed.

As mentioned before, an important assumption of the method of iodine conservation is that all absorbers relevant to the system under study are accounted for. Depending on the complexity of the chemical mechanism, the number of different product molecules increases with time. Therefore this assumption will become more difficult to fulfil the larger the time interval of data. Conversely, this limitation is also an important means for checking the reliability of the model, i.e. provided no systematic structures occur in the residuals, the number of species complies with the assumption. The appearance of systematic structures in the residuals indicates missed absorbers. In addition the systematic shape of the residuals will mirror quite closely the temporal behaviour of the absorber, which is not included in the model. Similarly any artefacts present in a temporal behaviour used for an absorber will cause systematic structures in the residuals. This could be the case for time intervals close to the flash, where issues of temporal resolution relative to the rapid initial formation of IO or its excited species might be of importance.

Fig. 6 shows an example of the solution of Eq. (x). The residuals are distributed normally, supporting the assumption that all relevant absorbers are accounted for and the two curves of obser-

Table 4
Absorption cross sections obtained in this work

Molecule	λ (vac) [nm]	σ[a] [cm^2 molecule^{-1}]	σ [cm^2 molecule^{-1}]	FWHM [nm]
IO	427.19 ± 0.05 (4 ← 0)	(MIntAS correction before iodine conservation)	$(3.5 \pm 0.3) \times 10^{-17}$	0.12[b]
IO*	449.3 ± 0.2 (3 ← 1)	(2.1 ± 1.3)	$>(3.9 \pm 2.4) \times 10^{-17}$, $(4.5 \pm 0.5) \times 10^{-17}$[c]	0.35[b] 0.12[b,c]
IO**	484.9 ± 0.2 (1 ← 2)	(0.5 ± 0.4)	$>(0.9 \pm 0.7) \times 10^{-17}$, $(6.0 \pm 0.5) \times 10^{-17}$[c]	0.35[b] 0.12[b,c]
OIO	549.3 ± 0.1 (0,5,1 ← 0, 0, 0)	(1.1 ± 0.3)	$(1.3 \pm 0.3) \times 10^{-17}$	0.35[b]
'Z'	356 ± 0.2 continuum		$>(7.8 \pm 1.2) \times 10^{-19}$[d]	1.3
'Y' (I_2O_2)	322 ± 0.2 continuum		$(1–8) \times 10^{-18}$[d]	1.3
'X'	373.2 ± 0.2 continuum		$(0.5–2) \times 10^{-18}$[d]	1.3

The measured OD for IO(4 ← 0) was MIntAS-corrected for effects of resolution and binning to an effective FWHM of 0.12 nm before usage of the method of iodine conservation. IO*, IO** and OIO were corrected afterwards with the appropriate scaling factors (Table 3). For I_2O_2 and 'Z' no resolution or binning dependent correction has been applied as they are continuous smooth absorptions. Note that for I_2O_2 only an estimated value can be given. The uncertainties are one standard deviation for each set of results.

[a] Result from iodine conservation with MIntAS correction to be applied afterwards by scaling.
[b] FWHM of MIntAS corrected cross section.
[c] Based on the cross section for (4 ← 0) at 0.12 nm FWHM and the Franck-Condon factors by Rao et al. [50].
[d] cm^2/iodine atom.

vation y and prediction coincide. In addition, the iodine column amount for each individual absorber is plotted.

As a further measure to investigate the possibility of unaccounted missing absorbers or artefacts, the following strategy was used. A starting point in time was chosen, which was assumed to be sufficiently remote from the flash to be free of artefacts. From there, an initial time window was selected and with the data from that window a first solution to the Eq. (x) was calculated. Then the interval was increased and a new solution to Eq. (x) was calculated. This procedure was repeated until the whole time interval of available data was covered. This produces a series of estimates for the absorption cross sections. Plotting the sets of results for absorption cross sections obtained in this way against the length of the used time interval provides a measure for the dependence of the obtained results. In the ideal case the solutions should produce a horizontal graph for each absorber's cross section. This criterion is referred to as "convergence on a horizontal plateau". Two reasons could cause deviations from this. Firstly, if the time interval does not contain significant information about one or more absorbers, because for example their OD is zero or close to zero within the selected interval, then the normal matrix of the system ($\boldsymbol{A}^T\boldsymbol{A}$) will become poorly conditioned or even singular. The results will show significant scatter and unsystematic behaviour. This is shown in Fig. 7, where results for a dataset of group 3 (see Table 2) are plotted. Under the conditions of group 3 the chemistry is very rapid (large O_3 and I_2 concentrations), and therefore the formation of further unaccounted species can be expected. The solutions behave erratically up to a fitting interval length of 1.5 ms (corresponds 75 data points). For fitting interval lengths between 1.5 ms (∼75 data points) and 4.2 ms (∼200 data points) the results for all absorbers are well behaved, implying that all

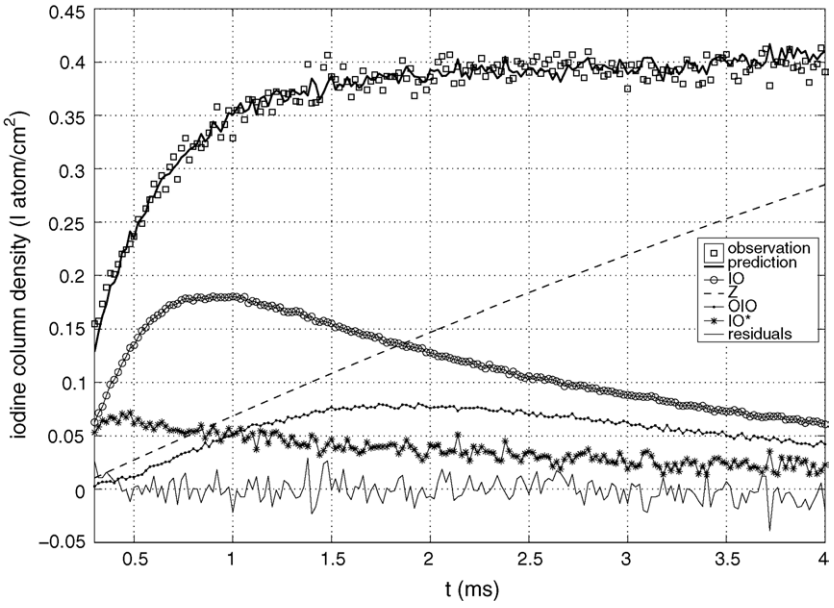

Fig. 6. Example of solution of Eq. (x) (conservation of iodine). The sum of the "iodine column density" of individual iodine containing species (curves in the lower half) must equal the observations for each point in time (top curve). The multivariate linear regression reproduced the observations accurately (top curve, open squares). At the bottom the residuals are plotted. Note that the time behaviour of 'Z' has been smoothed by polynomial fitting.

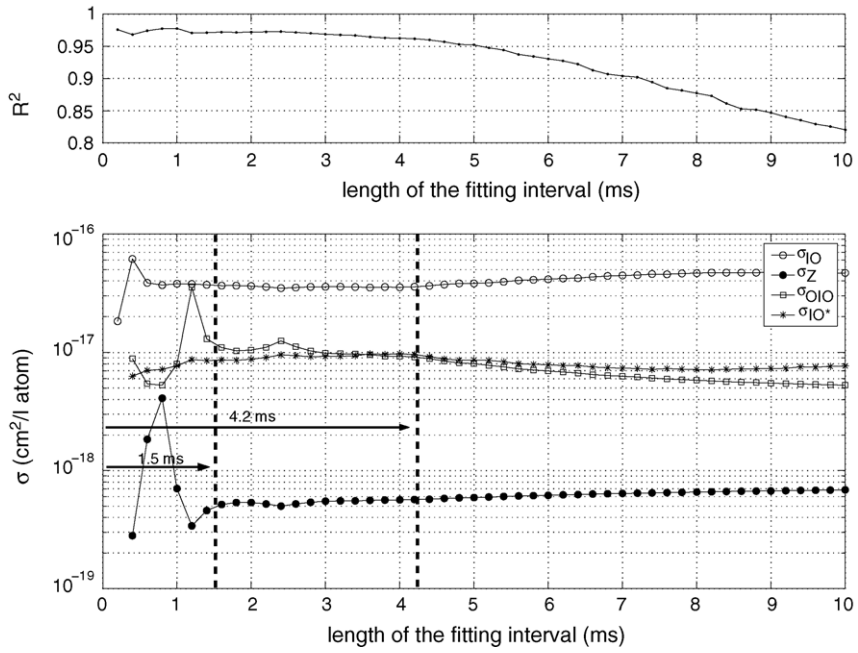

Fig. 7. An example for applying the method of iodine conservation to a data set is shown. Solutions to the iodine conservation model are calculated for different sizes of the fitting time interval. In the lower panel, from left to right, each "column" of points represents one individual solution of Eq. (x). The obtained cross sections are plotted against the length of the used time window providing a measure for the consistence of the obtained solutions. The corresponding correlation coefficients are plotted in the upper panel. Note that for fitting interval lengths between 1.5 ms (~75 data points) and 4.2 ms (~200 data points) the solutions are to a considerable degree constant ("horizontal plateau"). For windows larger than 4.2 ms the cross sections start to deviate from a constant behaviour, indicating the presence of unaccounted absorbers. Similarly, the corresponding correlation coefficients star to decrease.

absorbers are well defined by the observational data. Beyond window size of 4.2 ms the solutions start to deviate indicating that some further absorption might be missing. The corresponding correlation coefficients are plotted in the upper panel, and also indicate a poorer fit as the fitting time interval increases.

The condition of the normal matrix ($\boldsymbol{A}^{\mathrm{T}}\boldsymbol{A}$) is the key to whether the system can be solved or not. Collinearity impedes the separate solution of IO^*, IO^{**} and 'X', because their temporal behaviours are similar. Also collinearity between ground state IO and IO^* occurred. As a consequence an excited IO is fitted which comprises IO^*, IO^{**} and 'X'. This is an improvement upon the common practice, where ground state and vibrationally excited IO are treated as one absorber. Further, the different temporal behaviours will affect mainly the early time intervals, so that testing the convergence to horizontal plateaus as shown in Fig. 7 provides a measure to estimate the reliability of this approximation. To overcome collinearity problems between ground state IO and any of the excited species of IO, Eq. (x) was solved including IO(3 ← 1) or alternatively IO(1 ← 2). Whenever both alternatives converged to a set of results, cross sections for the remaining absorbers were averaged. If only one version produced results, these were used. As a result of collinearity the absorption cross sections obtained for IO^* and IO^{**} with the iodine conservation approach are effective or combined absorption cross sections of several species, and as a consequence only lower limits. However it is possible to obtain better estimations for the absorption cross sections of vibrationally excited IO by considering the Franck–Condon factors determined by Rao et al. [50]. Assuming comparable band shape for (4 ← 0), (3 ← 1) and (1 ← 2), the peak cross sections of the IO(3 ← 1) and IO(1 ← 2) bands should be about 0.116/0.091 ≈ 1.27 and 0.155/0.091 ≈ 1.70 larger than that of (4 ← 0). This yields estimated cross section of $\sigma_{IO(3\leftarrow1)} = 4.5 \times 10^{-17}$ cm^2 molecule^{-1} and $\sigma_{IO(1\leftarrow2)} = 6 \times 10^{-17}$ cm^2 molecule^{-1}.

Another way to estimate the peak cross section of the IO(3 ← 1) band is to assume that thermal equilibrium is reached. This is supported by the fact that after some milliseconds the ratio $a_{IO(3\leftarrow1)}/a_{IO(4\leftarrow0)}$ reaches a constant value. There is also observational evidence that as the pressure increases the channels of the IO self-reaction producing iodine atoms are reduced. This implies that at the highest pressures few I atoms are produced and the recycling is stopped in such a way that no more IO is produced. On the other hand higher pressure facilitates IO^* deactivation by collisional quenching. According to Boltzmann, the ratio of the number of molecules in the first excited state to that in the vibrational ground state at 298 K is $q = [IO^*]/[IO] = 0.04$. As a result, $\sigma_{IO(3\leftarrow1)} = \sigma_{IO(4\leftarrow0)} a_{IO(3\leftarrow1)}/(q a_{IO(4\leftarrow0)}) \leq 5.2 \times 10^{-17}$ cm^2, which is in very good agreement with the previous estimation. This is an upper limit because $q \geq 0.04$. The same procedure could be applied to IO(1 ← 2), but this absorption is under our detection limit when the equilibrium concentration is reached ($q = 0.002$).

If I_2O_2 is included the model for those data sets where it was observed (see Section 4.2.1) collinearity also caused problems. This could be identified as being a result of correlation in the temporal behaviours of OIO, 'Z' and I_2O_2. Effectively combining the behaviour of 'Z' and I_2O_2 (by neglecting the modelled curve of I_2O_2) solved the problem of collinearity. However from a priori chemical knowledge about the expected thermal decay of OIO and I_2O_2, OIO is expected to have a larger concentration

at shorter reaction times. As a result, the OIO cross section was determined at shorter time intervals (according to the criterion of convergence on a horizontal plateau) together with the cross section of 'Z'. An estimate of the absorption cross sections of 'X' and I_2O_2 has been obtained by fitting at larger time intervals the residuals of the observational vector when contributions of IO, IO^*, IO^{**}, OIO and 'Z' are removed. In Eq. (vii) all terms but the two corresponding to 'X' and 'Y' are moved to the left hand side. The new observational vector is the column density per iodine atom of all species but 'Y' and 'X'. Again a MLR is applied and estimates of the absorption cross sections of 'X' and I_2O_2 are obtained. This result in estimated absorption cross sections in the range between 0.5×10^{-18} and 2×10^{-18} cm^2 I $atom^{-1}$ for 'X', and between 1×10^{-18} and 8×10^{-18} cm^2 I $atom^{-1}$ for I_2O_2. Note that these two estimated ranges are the only results depending on the proposed time behaviour of I_2O_2.

The averaged results are summarized in Table 4.

5. Discussion

5.1. Consistency and independence of the determined absorption cross sections

The results listed in Table 4 are averages of individual results, obtained under a variety of different pressures and mixing ratios. To investigate their reliability the dependence on the parameters pressure, initial $[I_2]$ and initial $[O_3]$ were examined. No significant dependence on these parameters has been found (Figs. 8 and 9). Although absorbers 'X' and I_2O_2 and either one or the other of vibrationally excited IO^* or IO^{**} had to be neglected from the iodine conservation algorithm because of collinearity problems, the results obtained for IO($4 \leftarrow 0$) and

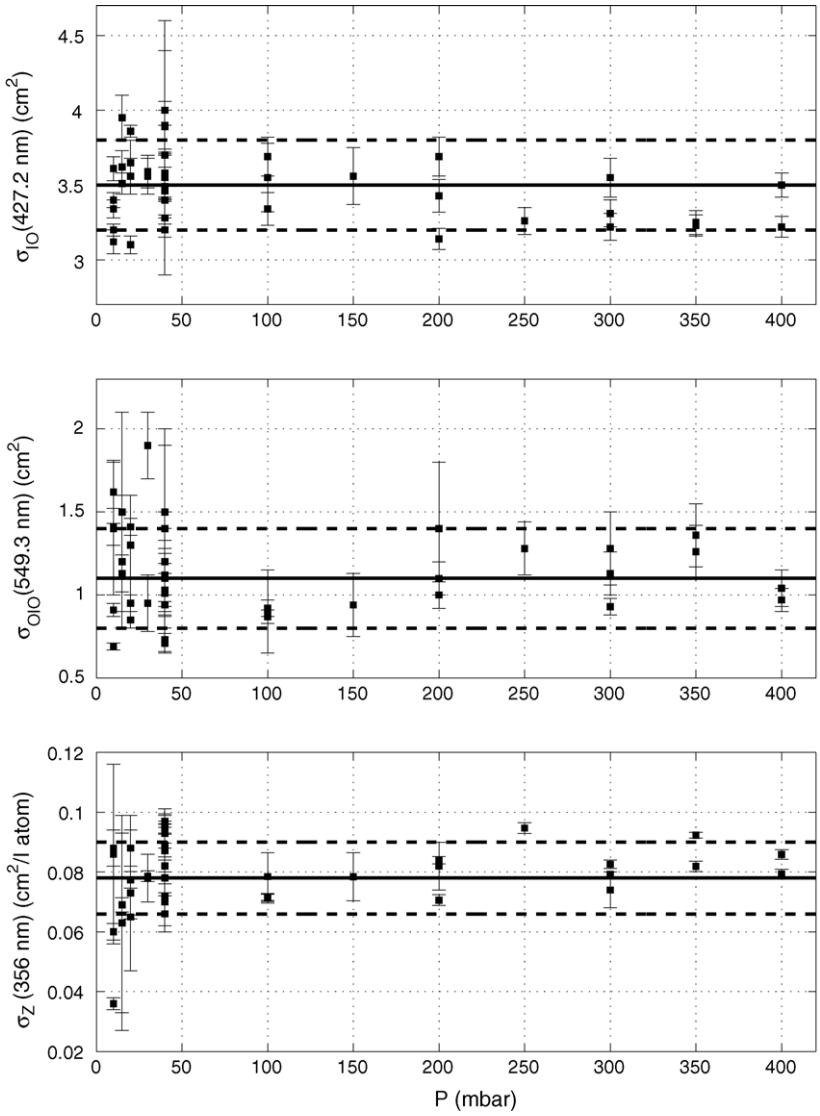

Fig. 8. Results for cross sections obtained from individual data sets by the method of iodine conservation are plotted against overall pressure present in the individual experiment. This provides a measure for sensitivity of the method to changed conditions. To avoid misunderstandings: Even though cross sections under certain conditions can display a pressure dependence as such, in the present context this is not of concern. Here the dependence of the method and its results on changed chemical and physical conditions, which in turn influences the partitioning between different species, is of concern. Please also note that the cross sections for OIO displayed in the central panel are not corrected for resolution effects. The correction is applied to the mean value by using the appropriate scaling factor shown in Table 3 (see discussion in Section 4.3). The solid horizontal line indicates the average and the dotted lines the interval defined by one standard deviation.

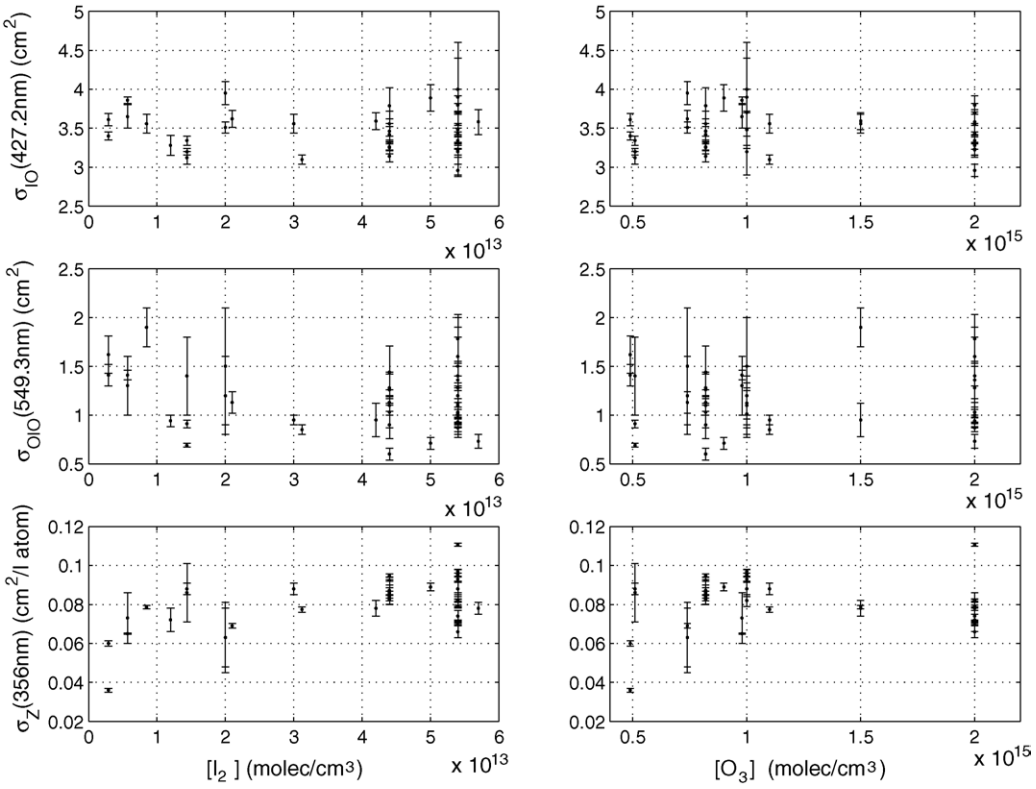

Fig. 9. The dependence of cross section results obtained for the individual data sets on initial $[I_2]$ and $[O_3]$ present in the experiment is examined. No significant dependences can be observed.

OIO(0, 5, 1 ← 0, 0, 0) are consistent and stable across the range of conditions used. The concept of iodine conservation results in the absorption from neglected species being combined to produce an effective cross section for a new combination parameter. Both neglected 'X' and IO^{**} behave in time similar to the corresponding curve of excited IO considered in the solution. Therefore the cross section estimate obtained in any of the two alternative solutions (either with OD of IO(3 ← 1) or IO(1 ← 2)) will underestimate the true cross section.

No LIF has been observed in previous works for IO(3 ← 1) (see [49]), indicating that it is a diffuse band. For IO(1 ← 2) no rotational structure is expected, as a result of no LIF from (1 ← 0) or (1 ← 1). By assuming a band profile similar to (4 ← 0) for these excited IO species, their cross sections can be estimated.

I_2O_2 and 'Z' have similar temporal behaviour. Therefore it can be expected that missing contributions from I_2O_2 are partly compensated in the effective 'Z' leading to an underestimation of its cross section.

In summary, in spite of the limitations imposed by collinearity between species, solution of the reduced data sets enables an independent, simultaneous and consistent determination of cross sections of ground state IO, and OIO, together with lower limits for the absorption cross sections of 'Z', IO^*, and IO^{**}. In addition we have calculated the IO^* and IO^{**} cross sections. The fact that for some data sets convergence to horizontal plateaus is achieved and in others not illustrates that collinearity is also linked to the chemical mixture, which changes the relative shape and the relative importance of individual temporal behaviours of absorbers. Alternative possibilities to solve the system of linear equations iteratively need to be investigated. Solution by use of perturbation theory could provide a means to overcome problems caused by collinearity. In the present work this is not pursued further, but left to future studies.

5.2. Comparison and analysis of published absorption cross section for iodine oxides

5.2.1. IO absorption cross sections

In this section the effects of instrumental resolution and line shape, the wavelength selected for the determination, effects of vibrationally excited IO, the absorption cross section of I_2 and kinetic hypotheses used in previous studies are discussed.

5.2.1.1. Effect of resolution. A significant number of measurements of the absorption cross section of IO have been published (Table 1). However the scatter among the resultant absorption cross sections is considerable. Taking the spectral resolution into account brings the one determination having a resolution poorer than 0.3 nm FWHM [34] into a better agreement with the rest. In Fig. 10 the available results are plotted as a function of resolution. The effect of resolution on the apparent peak height of the IO(4 ← 0) transition has been studied in Spietz et al. [47,51] by direct measurement (solid black line). The line shows the relative change of peak height with resolution, being scaled such that it is roughly centred within the available data. In this sense its vertical position is arbitrary, but its shape indicates that for our instrument line shape (ILS) the effect of resolution does not explain the

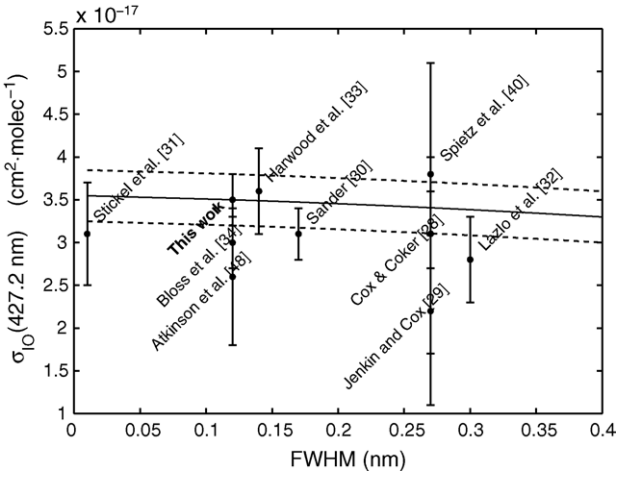

Fig. 10. Effects of resolution and binning can not explain the scatter among the published results for the IO ground state absorption cross section. The slightly inclined solid line shows the effect of resolution and binning on the IO(4 ← 0) band as determined in our measurements. The filled squares are a collection of published cross sections along with error bars and reference.

scatter of the available data. A down scaling of ∼3% is expected when reducing the resolution from 0.12 to 0.27 nm FWHM (see Fig. 11). It can be argued that the shape of the particular ILS determines the shape of the recorded spectra, as shown in Fig. 11, where our measured IO(4 ← 0) band at 0.27 nm FWHM is compared with the result of convolving our measured IO(4 ← 0) band at 0.12 nm FWHM with a 0.27 nm FWHM Gaussian ILS. However, the scaling factor resulting from a Gaussian ILS does not explain the difference between the absorption cross sections of [28,29] measured at 0.27 nm FWHM and the cross section of [33] measured at 0.14 nm FWHM. The agreement of our characterisation of instrumental effects with the results obtained by Crowley et al. [21] with a different detector indicates that for moderate resolutions (less than 0.3 nm) the shape of the ILS does not play a significant role and that instrumental effects are of secondary importance in explaining the scattering of published values.

5.2.1.2. Consequences of selecting different wavelengths for the determination of σ(4 ← 0). Durie et al. determined the band head of IO *in absorption* [26] to be at 426.98 nm (they do not state if this is for vacuum or for air), and *in emission* [27] at 426.82 nm (air). Rigorously speaking, the band heads of the $A^2\Pi_{3/2} \leftarrow X^2\Pi_{3/2}$ subband system of IO are defined by the vertex of the R branch Fortrat parabola (see e.g. Durie et al. [27], Newman et al. [52]). The band head is well defined for those bands presenting rotational structure like IO(2 ← 0), but in the case of diffuse bands the concept of band head is ambiguous. According to Herzberg [53], the band head is the sharp edge of the *spectral* structure where the intensity falls suddenly to zero, and not the maximum. The studies by Cox and Coker [28] and Jenkin and Cox [29] determined the IO cross section at the band head at 426.9 nm, which explains why their cross sections are in general lower than the rest. It can be assumed that this wavelength is given for air, because if it were for vacuum the absorption would have been very small, as shown in Fig. 11. The wavelength reported in [28,29] is located indeed on the steep flank of the band and a small variation in wavelength leads to a large variation in the absorption cross section.

More precision in the wavelength reported would be required to transfer the values from [28,29] accurately to our stan-

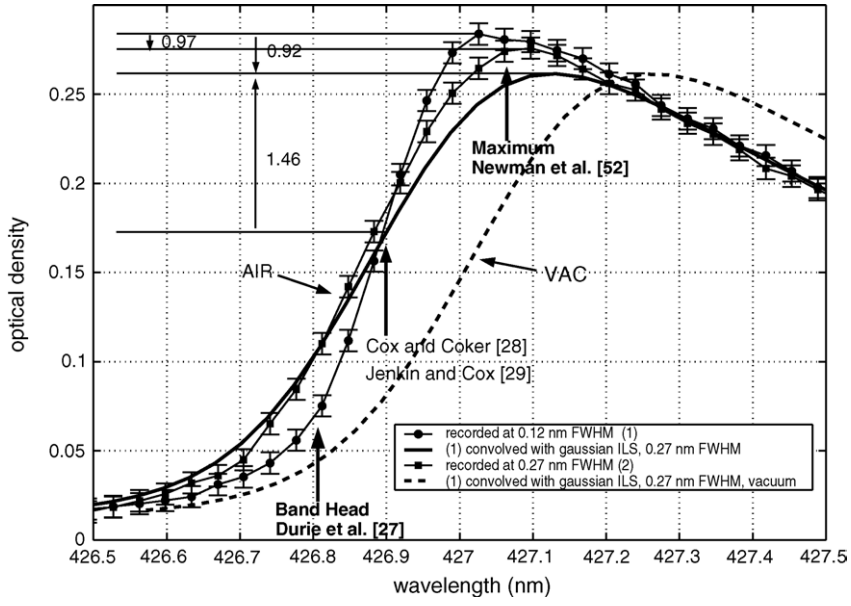

Fig. 11. Effects of instrument resolution, line shape and wavelength shift. Our measured IO(4 ← 0) band at 0.27 nm FWHM (circles) is compared with the result of convolving our measured IO(4 ← 0) band at 0.12 nm FWHM (squares) with a 0.27 nm FWHM Gaussian ILS (result: solid line). The expected reduction in the peak absorption is ∼3% with the same ILS. For a Gaussian ILS the reduction is ∼7%. The figure also shows that the strong dependence of the absorption cross section on wavelength in the step flank of the band introduce large uncertainties in those determinations of σ made in this spectral range if the accuracy in the wavelength calibration is not good enough. The wavelength axis is for air for all curves but for the dashed one, which is the same curve as the solid one but in the vacuum wavelength axis.

dards. The scaling factor between the (resolution dependent) cross section at 426.9 nm and the peak cross section is ~1.5, which yields an unreasonably large cross section for [28]. To illustrate the effect of inaccuracies in wavelength, a measurement at 426.95 nm (air) has been considered, which would produce a scaling factor of ~1.2. This results in a modified value of 3.7×10^{-17} cm^2 molecule^{-1} for [28] and 2.6×10^{-17} cm^2 molecule^{-1} for [29].

Sander [30] determined the cross section at 427.2 nm, after he had made sure that at this wavelength no part of the monochromator response extended beyond the band head. The CRD spectrum of Newman et al. [52] has its peak absorption at 427.20 nm (vacuum) in agreement with our observations. Most studies report the cross section at this wavelength although some authors refer wrongly to it as the band head. In addition, in some of these studies it is unclear whether the convention adopted is to give wavelengths in vacuum or in air. The uncertainty introduced by such ambiguity is illustrated in Fig. 11, where one of the curves is plotted in a vacuum wavelength axis.

5.2.1.3. Dependence on different I_2 cross section reference data. Among the lower results those of Laszlo et al. [32] and Atkinson et al. [48] are systematically linked (see Section 4.4). In the determination of an absolute cross section for IO Laszlo et al. calibrated the concentration of IO in their experiment by using a cross section for I_2 of $\sigma_{I_2}(530\,\text{nm}) = 2.56 \times 10^{-18}$ cm^2 molecule^{-1} published by Calvert and Pitts [54]. Our own determination of the I_2 cross section proved the results by Tellinghuisen [35] to be highly reliable (see [37] and the discussion therein). Another recent study by Saiz-López et al [36] also has confirmed these results. At 530 nm Tellinghuisen reports a significantly larger iodine cross section of $\sigma_{I_2}(530\,\text{nm}) = (3.1 \pm 0.1) \times 10^{-18}$ cm^2 molecule^{-1} at low resolution. Use of these cross sections changes the calibration of IO concentration in the data by Laszlo et al. and after rescaling their result, this yields $(3.4 \pm 0.6) \times 10^{-17}$ cm^2 molecule^{-1}. In addition it should be noted that the determination of I_2 concentration in the ro-vibronic region above 500 nm as a result of its rich ro-vibronic structure is intrinsically more difficult than at 500 nm. Results depend on good knowledge of the resolution and pressure. Therefore even after correction of the I_2 cross section the results have probably additional systematic errors.

5.2.1.4. Effects of vibrationally excited IO. The amount of vibrationally excited IO depends on two factors

(a) collisional quenching and
(b) presence of permanent sources of IO in the experiment (e.g. reactions (1) and/or (4)).

Comparing the molecular modulation or modulated photolysis studies [28,29] provides evidence for the presence of excited IO. The study at high pressure ([28], 1013 mbar) yields a larger cross section of 3.1×10^{-17} cm^2 molecule^{-1}, whereas that at low pressure ([29], 10–100 mbar, even though they did not mention the observation of IO*) yielded a significantly smaller cross section of 2.2×10^{-17} cm^2 molecule^{-1}. This pressure dependence can be understood easily in terms of a non-equilibrium distribution of IO present during the modulation cycle and caused by a permanent IO source. Lower pressure experiments have larger amounts of IO($X^2\Pi_{3/2}$, $v'' > 0$). Thus the amount of IO is overestimated and σ_{IO} underestimated. No attempt to estimate the systematic error related to IO* in the cross section of Jenkin and Cox [29] has been made, because the absorption due to IO* was not monitored.

The same effect is probably observed in the work of Stickel et al. [31], even at atmospheric pressure. Their system used both reactions (1) and (4) as IO sources, in such a way that iodine atoms are permanently recycled in the IO self-reaction and react subsequently with O_3. Therefore, there is also a permanent source of IO($X^2\Pi_{3/2}$, $v'' = 0$) and IO($X^2\Pi_{3/2}$, $v'' > 0$). The pressure is rather high, but the decay of IO is slow, as their figures show, and, unlike in our system, IO does not have time to relax to the equilibrium distribution on the time scale of the experiment. The ratios for $a_{IO(3\leftarrow1)}/a_{IO(4\leftarrow0)}$, obtained from the spectrum of [31] and at the highest pressure in our study (400 mbar) are, respectively ~0.15 and ~0.06, implying that the Stickel et al. system is not in local thermal equilibrium and contains much more IO($X^2\Pi_{3/2}$, $v'' > 0$) relative to IO than our system. Based on this ratio and the absorption cross section of IO* determined in this work, a 10% correction upwards of the absorption cross section of [31] has been estimated (3.4×10^{-17} cm^2 molecule^{-1}).

5.2.1.5. Mechanistic approaches: possible effects of parameterisation or dependence on kinetic reference data. The IO cross section which was determined earlier in our laboratory ($\sigma_{IO}(4 \leftarrow 0) = (3.8 \pm 0.2) \times 10^{-17}$ cm^2 molecule^{-1}, Spietz et al. [40]) was the result of a complex fit to curves of the temporal behaviour of IO, OIO, I_2 and O_3. These had been recorded one after another with up to 10 h between the first and last recording. In spite of the well known deposition in the course of reaction, the chemical conditions in this system had to be assumed to be constant during that period to enable analysis. Our recent studies demonstrated that due to the accumulation of deposit and also to its photolysis this assumption is a potential source of error. Therefore the error limit given in [40] must be regarded as too optimistic. The cross sections were determined using the commercial FACSIMILE software package [55] and a complex chemical mechanism. The concentration of IO therefore depends on the knowledge of a comparatively large number of kinetic rate coefficients. In addition the effect of vibrationally excited IO was not taken into account. Re-evaluation of the data with systematic weighting by the available error estimates yields $(3.4 \pm 0.8) \times 10^{-17}$ cm^2 molecule^{-1}.

The work of Stickel et al. [31] relied on a number of rate coefficients among which the overall rate coefficient for the IO + IO self-reaction was used at 6×10^{-11} cm^3 molecule^{-1} s^{-1}. More recent studies of this reaction rate coefficient yield larger values. This would increase the result of [31] making it a lower limit.

Harwood et al. [33] determined $\sigma_{IO}(4 \leftarrow 0)$ in three different chemical systems (($N_2O + h\nu$) + CF_3I, ($O_3 + h\nu$) + I_2, ($N_2O + h\nu$) + I_2). The first chemical system was found to produce the results with smallest uncertainty. This system relies on the knowledge of the yield Φ of IO in the reaction of O + CF_3I. In

the analysis of their experimental data obtained at 420 mbar Harwood et al. [33] used a value of $\Phi = 0.86 \pm 0.06$ and quoted Gilles et al. [56] (in fact the value published in [56] was 0.83 ± 0.09, obtained at 130 mbar being independent of temperature). Bloss et al. [34] examined the dependence of Φ on pressure and temperature and found no significant pressure dependence at 295 K (they also quoted [56], although used a value of $\Phi = 0.845$). Therefore, in both studies approximately the same value for Φ was used. The differences between [33] and [34] studies were:

(i) Significantly larger concentrations of IO were used in the study of Bloss et al. [34] and consequently faster losses by the self-reaction.
(ii) Bloss et al. [34] did not model losses near the initial peak absorption of IO, as was done by Harwood et al. [33]. Therefore their result should underestimate the true cross section.

In [33] the modelling of possible losses opposed to the simple stoichiometric conversion assumption led to changes of less than 10%. In [34] concentrations were larger and removal of IO faster. Assuming a 10% correction, the cross section of [34] would be 3.3×10^{-17} cm^2 molecule^{-1} in better agreement with our cross section and that of [33].

5.2.2. OIO absorption cross sections

A lower limit of 0.4×10^{-17} cm^2 molecule^{-1} for the absorption cross section of the OIO (0, 5, 1 ← 0, 0, 0) transition had been previously obtained in our laboratory [40]. In contrast, the lower limit of 2.7×10^{-17} cm^2 molecule^{-1} obtained by Ingham et al. [19] is in disagreement with our determination. It was calculated by assuming branching ratio 1 for the OIO + I channel of the IO self-reaction and ignoring losses of OIO. It is explicitly based in the time resolved absorption of IO and the time resolved differential absorption of OIO (549.l − 553.0 nm) shown in one of the figures of [19]. If the time axis is plotted correctly and the curves displayed correspond to each other as indicated, it is easy to see that a decrease of IO $\Delta a_{\mathrm{IO}(427.2\ \mathrm{nm})} \approx -10^{-2}$ between 0.25 and 0.75 ms corresponds to an increase of OIO $\Delta a_{\mathrm{OIO\ diff}} \approx 10^{-3}$. According to our understanding $\sigma_{\mathrm{OIO\ diff}} \geq \sigma_{\mathrm{IO}(427.2\ \mathrm{nm})}\, 2\, \Delta a_{\mathrm{OIO\ diff}} / |\Delta a_{\mathrm{IO}(427.2\ \mathrm{nm})}| \approx 3.6 \times 10^{-17} \times 2 \times 10^{-3} \times 10^{2} = 7.2 \times 10^{-18}$ cm^2 molecule^{-1}, where the IO cross section of [33] has been used. This results in an estimated lower limit of $\sigma_{\mathrm{OIO}(0,5,1\leftarrow 0,0,0)} \geq 1.2 \times 10^{-17}$ cm^2 molecule^{-1}, in contradiction with the result of [19]. A reason for this discrepancy could be that Ingham et al. [19] take $[\mathrm{IO}](t = 0) = 5 \times 10^{12}$ molecule cm^{-3}, although Fig. 8 of [19] shows that $[\mathrm{IO}](t = 0) = 0$. A maximum value of $[\mathrm{IO}] = 5.3 \times 10^{12}$ molecule cm^{-3} is reached after 0.25 ms. Parallel to this increase in IO, an increase of 0.002 in the OIO differential optical density is observed. If the initial concentration is assumed to be 5×10^{12}, then the initial time must be shifted to approximately $t = 0.25$ ms. The half life for the IO decay is correspondingly shifted to 1.25 ms. The concomitant OIO production between 0.25 and 1.25 ms can be estimated in 1.25×10^{12} molecule cm^{-3} if a 100% yield for I + OIO is assumed, as argued in [19]. This corresponds to the change in optical density observed *in this interval* (∼0.001), which is a factor 3 smaller than the change observed between $t = 0$ and 1 ms. Thus, a lower limit for the differential absolute absorption cross section of about 6×10^{-18} cm^2 molecule^{-1}is obtained, in agreement with our own analysis.

The range published by Bloss et al. [34] (see Table 1) is in reasonable agreement with our value. Plane et al. [22] report a value of $(1.5 \pm 0.2) \times 10^{-17}$ cm^2 molecule^{-1} at (0, 4, 1 ← 0, 0, 0), (i.e. 1.57×10^{-17} cm^2 molecule^{-1} for the (0, 5, 1 ← 0, 0, 0) band) obtained with a 0.0025 nm FWHM binned CRD system, while J. Crowley (personal communication, 2005) report $(1.2 \pm 0.3) \times 10^{-17}$ cm^2 molecule^{-1}. Both values are in reasonable agreement with the relevant OIO absorption cross sections determination from our study within the experimental error limits.

5.2.3. Broad band absorbers

Cox and Coker [28] observed a broad band absorption between 220 and 500 nm and they attributed it to a light scattering aerosol product, based on its non-linear growth and wavelength dependence. According to their results the relationship between $\log_{10}(a)$ and $\log_{10}(\lambda)$ is linear with slope −4, as expected for scattering by particles with radius much smaller than the wavelength (Rayleigh regime, $r \ll 0.2\ \mu$m). For the UV broad absorption observed in our system, no such linear dependence is found. In the spectral range between 340 and 435 nm this absorption has been linearly factorized and attributed to overlapping absorptions I_2O_2 and 'Z', as explained in Section 4.2.1. In addition the reproducibility of the absorption and the analogous relative spectral position of higher chlorine and bromine oxides results in the conclusion that in our study broad band absorptions of gases are observed. Cox and Coker [28] measured on a longer time scale (60 s) and produced continuously iodine oxides by modulation. Time scales and amount of iodine oxides produced were appropriate for aerosol production. Our measurements are not longer than 30 ms and the source reaction is limited by the presence of iodine atoms, which after about 5 ms are completely removed by reaction with O_3. The deposition at the walls in our study is however evidence for the production of smaller cluster molecules, which would scatter at shorter wavelengths.

Sander [30] also observed broad band absorption in the UV between 230 and 300 nm in his O_3/I_2 system on a time scale one order of magnitude larger than ours (∼100 ms). Without ruling out the possibility of aerosol, he attributed this absorption to a single gas phase species. By assuming a 100% product yield from the IO self-reaction he put an upper limit of 2.6×10^{-17} cm^2 molecule^{-1} to the cross section at 220 nm (∼3×10^{-18} cm^2 molecule^{-1} at 300 nm). By comparing the formation of the product and the decay of IO he concluded that the time scale for complete formation of the product is considerably longer than for IO disappearance, what is indicative of a multistep product formation mechanism. A further argument against I_2O_2 is that it would thermally dissociate on a shorter time scale, according to ab initio quantum calculations performed by Plane et al. [22] and Mishra et al. [57].

Bloss et al. [34] observed a broad absorption in the UV (360–460 nm) over a time scale of several milliseconds behaving in a manner similar to the one we have measured. They

assigned this absorption to I_2O_2 based on its kinetic behaviour and derived an upper limit of 2×10^{-18} cm^2 molecule^{-1} for its absorption cross section at 340 nm based on a 100% yield from the IO self-reaction. This is in qualitative agreement with the upper limit of Sander (extrapolation to 300 nm was not possible in this case). These values are also in qualitative agreement with our value at 340 nm of $(1.0 \pm 0.2) \times 10^{-18}$ cm^2 I atom^{-1}. However in our case the temporal dependence curves observed cannot be reproduced by IO second order kinetics (Fig. 3), even if potential sinks such as dissociation or iodine abstraction are considered.

The kinetic behaviour of 'Z' is more consistent with its being assigned to the molecule I_2O_3, formed by the reaction of IO with OIO in a pressure dependent reaction, although this is not completely consistent with the decay of OIO. I_2O_3 is a stable higher iodine oxide according to ab initio quantum calculations performed by Plane et al. [22]. Some other possibilities have been explored to make a kinetic assignment of 'Z'. The temporal behaviour of OIO can be modelled by its self-reaction, followed by the reaction of OIO with a product of its own self-reaction. However, 'Z' does not fit well to any of the hypothetical products generated in this scheme. A pseudo first order decay of OIO is consistent with both observed curves although it is not clear which species could participate in such reaction. The possibility of the reaction OIO + O_3 has been explored and rate coefficients of the order of magnitude of 10^{-13} cm^3 molecule^{-1} s^{-1} have been obtained. However, this reaction is not compatible with the observation of OIO in the MBL. Saiz-López et al. (personal communication, 2005) have calculated an upper limit to this reaction rate of 5×10^{-14} cm^3 molecule^{-1} s^{-1} by using their atmospheric chemical model for the coastal MBL. Clearly more kinetic studies are required to make a statement in this sense. Also spectroscopic evidence is required, which could be obtained by investigating the rotational-vibrational structure (see Chase [58] and references therein) expected for the higher iodine oxides in the mid and far infrared. The discussion of the assignment of 'Z' is left for further work. Nevertheless, the absorption cross section we report here is independent of the kinetic assignment and is given consequently as an absorption cross section per iodine atom. In Section 4.2.1 evidence is provided that I_2O_2 explains the absorption deeper in the UV initially denominated as 'Y'.

The identity of the short lived absorber 'X' is also intriguing. The following reactions may produce such a transient absorption shortly after the flash:

$$I + O_2 + M \leftrightarrow IOO + M \quad (9)$$

$$I + O_3 + M \leftrightarrow IO_3 + M \quad (10)$$

$$I + O_3 \rightarrow IO(X^2\Pi_{3/2}, v'' > 0) + O_2 \quad (1b)$$

$$I + O_3 \rightarrow IO(X^2\Pi_{1/2}) + O_2 \quad (11)$$

Although attractive as the observed broad band spectra appears similar to that observed in the matrix by Maier et al. [59], the possibility of the absorption being by IOO has been excluded at this time, because photolysis of I_2/O_2 mixtures (i.e. the same mixtures excluding O_3) do not provide any evidence for the short lived transient. A potential explanation for the observed transient absorption would be that it belongs to an IO_3 molecule, formed during the time of high I concentrations at short reaction times. The IO_3 then subsequently dissociates to reform I and O_3.

Spectroscopic vibrational analysis has shown that the absorption does not originate from excited vibrational state $IO(X^2\Pi_{3/2}, v'' > 0)$. In contrast, a plausible explanation of the absorption attributed to 'X' is the $A^2\Pi_{1/2} \leftarrow X^2\Pi_{1/2}$ subband system. This assignment is discussed in the accompanying paper [41] about spectroscopy of iodine oxides.

5.3. Atmospheric relevance

Recent studies of IO (this work, [33], [21]) have resulted in a consensus about our understanding of its ground state absorption cross sections in the UV–vis. In the case of OIO, since its first observation in the gas phase in our laboratory, two upper limits and one determination of its absorption cross section have been reported ([19], [40], and [34]). The results of our work agree well with the latest results of other groups (Plane et al. [22], Crowley and Dillon, personal communication 2005). As a consequence of the exhaustive analysis of the literature values, the characterization of the instrumental effects, the separation of overlapping absorbers and the general reduction of uncertainties, the accuracy of the atmospheric retrieval of IO and OIO concentrations by absorption spectroscopy and of the photolysis rates will be significantly improved.

To illustrate the relevance of absorption cross section data in the study of atmospheric processes, the spectra shown in the accompanying paper [41] and the absolute scaling reported in the present work have been used to determine the photolysis rates of all species studied for a latitude of 40° at summer solstice as a function of altitude and zenith solar angle (SZA). Actinic fluxes at 1.3 nm FWHM resolution have been calculated with the radiative transfer model SCIATRAN [60] (for an introduction to the model see [61] and references therein) for a typical water surface albedo of 0.1, assuming a cloud free sky and a total ozone column of 330 DU. The use of unity quantum yield for IO and IO* can be inferred from LIF [49] and CRD [52] studies showing that dissociation from all ro-vibronic states in the upper electronic state occurs very rapidly. Moreover, Ingham et al. [19] measured a quantum yield close to unity for IO at 355 nm. For all broad band absorbers a unity quantum yield has been assumed. For OIO an upper limit of 0.1 has been considered based in the results obtained by Ingham et al. [19] (532 nm) and Plane et al [22] (562 nm). The results obtained are shown in Table 5.

The photolysis rates calculated for IO are in qualitative agreement with the values obtained by Lazlo et al. [32], Harwood et al. [33] and Bloss et al. [34]. Our results are smaller than those of [32,33], most likely as a result of the lower underlying continuum exhibited by the wavelength dependent absorption cross section reported in the accompanying paper [41]. Additionally, the spectra in [33] contain IO* bands. In general, the values reported here are in better agreement with those of Bloss et al. [34], whose spectrum presents the smallest difference to our spectrum in the continuum. In this case the smaller cross section of [34] at 427.2 nm (used to scale the IO spectrum) could

Table 5
Atmospheric photolysis rates (40°N, summer solstice, cloud free sky, albedo 0.1 and total ozone column of 330 DU) for relevant iodine oxides as a function of height and solar zenith angle

SZA	Photolysis rate (s^{-1})									
	0 km		5 km		10 km		20 km		30 km	
16°	0.18[a]	0.11[b]	0.22	0.14	0.23	0.14	0.23	0.14	0.23	0.14
	0.016[c]	0.042[d]	0.022	0.048	0.023	0.049	0.023	0.049	0.022	0.048
	0.024[e]	0.032[f]	0.037	0.040	0.041	0.040	0.041	0.029	0.039	0.025
40°	0.15	0.10	0.21	0.13	0.22	0.14	0.23	0.14	0.22	0.13
	0.013	0.038	0.020	0.046	0.022	0.048	0.022	0.048	0.021	0.047
	0.018	0.030	0.031	0.042	0.035	0.045	0.037	0.038	0.036	0.024
60°	0.11	0.08	0.18	0.12	0.20	0.13	0.21	0.13	0.21	0.13
	0.009	0.029	0.016	0.042	0.019	0.045	0.020	0.046	0.020	0.045
	0.010	0.021	0.020	0.037	0.025	0.042	0.030	0.042	0.030	0.04
80°	0.03	0.02	0.09	0.07	0.13	0.09	0.17	0.11	0.18	0.11
	0.003	0.009	0.006	0.027	0.010	0.033	0.015	0.038	0.016	0.039
	0.002	0.006	0.005	0.014	0.008	0.021	0.014	0.030	0.016	0.036

[a] IO.
[b] IO^*.
[c] 'X'.
[d] Upper limit for OIO.
[e] Lower limit for I_2O_2.
[f] Lower limit for 'Z' (it is assumed that 'Z' contains two iodine atoms).

explain our slightly larger photolysis rates. The partitioning of reactive iodine (IO_x) between I and IO is determined by the photolysis rate of IO and the rate of reaction (1), and a smaller photolysis rate implies a greater partitioning of IO_x as IO in the atmosphere. This implies a larger ozone destroying potential of the iodine chemistry if subsequent reactions of IO produce free I atoms without concomitant $O(^3P)$ formation.

In the case of IO^*, photolysis cannot compete with collisional quenching. For the MBL the quenching rate derived from our data is $\sim 5 \times 10^4\ s^{-1}$, while in the lower stratosphere is $\sim 3 \times 10^4\ s^{-1}$. This analysis also applies to 'X' if the assignment to $IO(X^2\Pi_{1/2})$ is correct and the decay observed (Fig. 3f) is also due to collisional quenching.

Most estimations reported in the literature for the photolysis rate of OIO [20,34] have been obtained by considering a unity quantum yield. The current understanding is that OIO is relatively photostable, although an upper limit for the quantum yield of about 0.1 is still high enough to make photolysis a main fate of OIO in the day time. Estimated values of reaction rates for the reaction of IO and OIO and for the self-reaction of OIO are about $2 \times 10^{-10}\ cm^3\ molecule^{-1}\ s^{-1}$ [22,62]. By assuming atmospheric mixing ratios of 5 and 0.5 ppt for IO and OIO, respectively [12] and a photolysis rate of $0.04\ s^{-1}$, the rate of removal by chemical reaction of OIO is approximately equal to the photolysis rate. This enables the participation of OIO in new particle formation [5–7] through a homogeneous heteromolecular nucleation mechanism even at day time. In this sense, the observation of higher oxides in the UV and the collection of solid deposits (I_2O_5) give evidence that some sort of clustering mechanism is taking place as well in our system.

For the higher iodine oxides only upper limits can be estimated due to the partial spectral coverage. Nevertheless, the actinic flux under 300 nm is small enough to consider these low limits as realistic approximations. Both I_2O_2 and 'Z' present mean lives with respect to photolysis of tenths of seconds. Again, estimated reaction rates for higher iodine oxides of the order of magnitude of $10^{-10}\ cm^3\ molecule^{-1}\ s^{-1}$ enable clustering to compete with photolysis.

6. Summary and conclusion

The method of iodine conservation has been successfully applied in the determination of absorption cross sections from time resolved flash photolysis of I_2 and O_3 mixtures with detection by absorption spectroscopy. Results have been obtained for ground state IO, vibrationally excited IO, OIO and in addition for three further UV absorptions, one of them tentatively assigned to I_2O_2.

$\sigma_{IO(4\leftarrow0)}(427.2\ nm) = (3.5 \pm 0.3) \times 10^{-17}\ cm^2\ molecule^{-1}$ at 0.12 nm FWHM is in good agreement with the recent published data. It is a cross section for the *ground state* $IO(4 \leftarrow 0)$ progression. It is not – as it has to be inferred from determinations, where vibrationally excited IO was observed but not considered in the calculations – an effective cross section accounting for IO in the electronic ground state ignoring the vibrational excitation. An *effective* absorption cross section for excited IO was determined relative to the $(3 \leftarrow 1)$ transition. Its value accounts *simultaneously for all* $IO(\nu' \leftarrow \nu'')$, with $\nu'' > 0$: $\sigma_{\text{eff}\,IO(3\leftarrow1)}\ (459.3\ nm) = (3.9 \pm 2.4) \times 10^{-17}\ cm^2\ molecule^{-1}$ at 0.35 nm FWHM. Based on Franck–Condon factors an absolute cross section for $IO(3 \leftarrow 1)$ valid for the $\nu'' = 1$ progression was determined relative to $\sigma_{IO}(4 \leftarrow 0)$, 0.12 nm FWHM: $\sigma_{IO(3\leftarrow1)}(459.3\ nm) = (4.5 \pm 0.5) \times 10^{-17}\ cm^2\ molecule^{-1}$ at 0.12 nm FWHM. Similarly, a value of $\sigma_{IO(1\leftarrow2)}(484.9\ nm) = (6.0 \pm 0.5) \times 10^{-17}\ cm^2\ molecule^{-1}$ at 0.12 nm FWHM for the $\nu'' = 2$ progression has been obtained.

After consideration of various effects the scatter between the available cross section data for IO could be reduced, resolving some of the inconsistencies. On the scale of the stated uncertainties most of the published results agree. Our result is somewhat larger than all others except that by Harwood et al. [33]. However the other values can be considered as systematic underestimations for reasons discussed above. The insensitivity of our method to experimental conditions, the dedicated consideration of vibrationally excited IO in our approach as well as the discussion of the compensation pattern for neglected absorbers was an attempt to minimise any underestimation of the IO absorption cross section. A weighted average of the (corrected) results at 298 K (bold case, Table 1) yields a value of 3.3×10^{-17} cm^2 molecule^{-1}. Considering only the scatter of the data used for averaging produces a standard deviation of $\pm 0.2 \times 10^{-17}$ cm^2 molecule^{-1}. Nevertheless, this average must still be considered as a systematic underestimation, as a result of the discussion above. The corrections introduced in some values must be also considered with care. Therefore, we recommend weighted average between the value of [33] and our own value: $(3.5 \pm 0.4) \times 10^{17}$ cm^2 molecule^{-1} at 427.2 nm (vac.). The inverse of the uncertainties have been used as weighting factors.

The cross section of OIO was found to be $\sigma_{\mathrm{OIO}(0,5,1 \leftarrow 0,0,0)}$ (549.3 nm) = $(1.3 \pm 0.3) \times 10^{-17}$ cm^2 molecule^{-1} at 0.35 nm FWHM, being in good agreement with the previous determination.

For the absorber 'Z' a lower limit σ (356 nm) $\geq (7.8 \pm 1.2) \times 10^{-19}$ cm^2 I atom^{-1} (σ(340 nm) $\geq (1.0 \pm 0.2) \times 10^{-18}$ cm^2 I atom^{-1}) has been determined. For the absorber tentatively assigned to I_2O_2, the absorption cross section at 322 nm is in the range from 1 to 8×10^{-18}cm^2 I atom^{-1}.

The main limitation to the method of iodine conservation is collinearity between OD temporal behaviours of absorbers. It appears promising to consider regularisation methods as well as approaches similar to perturbation theory to overcome this limitation.

7. Supporting information

The wavelength dependence of IO, OIO and I_2 absorption cross sections determined in the course of this work and the accompanying paper are available at www.iup.uni-bremen.de/gruppen/molspec/index.html.

Acknowledgements

The authors wish to thank Hilke Oetjen for helpful comments on the use of the radiation transfer model SCIATRAN. This work was partially founded by the German Space Agency (contract 50EP9207 'SCHIAMACHY' and project LVA 01/003), the European Union (contract EVK2-CT2001-00104 'THALOZ'), the EU-ACCENT Network of Excellence and the University and the State of Bremen.

References

[1] W.L. Chameides, D.D. Davis, Iodine: its possible role in trophospheric photochemistry, J. Geophys. Res. 85 (1980) 7383–7398.
[2] R.B. Chatfield, P.J. Crutzen, Are there interactions of iodine and sulphur species in marine air photochemistry? J. Geophys. Res. 95D (1990) 22319–22341.
[3] S. Solomon, R.R. García, A.R. Ravishankara, On the role of iodine in ozone depletion, J. Geophys. Res. 99 (1994) 20491–20499.
[4] S. Himmelmann, J. Orphal, H. Bovensmann, A. Richter, A. Ladstaetter-Weissenmayer, J.P. Burrows, First observation of the OIO molecule by time resolved flash photolysis absorption spectroscopy, Chem. Phys. Lett. 251 (1996) 330–334.
[5] R.A. Cox, W.J. Bloss, R.L. Jones, D.M. Rowley, OIO and the atmospheric cycle of iodine, Geophys. Res. Lett. 26 (13) (1999) 1857.
[6] T. Hoffmann, C.D. O'Dowd, J.H. Seinfeld, Iodine oxide homogeneous nucleation: An explanation for coastal new particle production, Geophys. Res. Lett. 28 (2001) 1949–1952.
[7] C.D. O'Dowd, J.L. Jimenez, R. Bahreini, R.C. Flagan, J.H. Seinfeld, M. Kulmala, L. Pirjola, T. Hoffmann, Particle formation in the marine atmosphere controlled by biogenic iodine emissions, Nature 417 (2002) 632–636.
[8] F. Wittrock, M. Eisinger, A. Ladstätter-Weißenmayer, A. Richter, JP. Burrows, Ground based UV–vis measurements of O_3, NO_2, BrO and OClO over Ny-Alesund (79°N, 12°E), in: J.A. Pyle, N.R.P. Harris, G.T. Amanatidis (Eds.), Air Pollution Research, vol. 56, Proceedings of the Third European Polar Ozone Symposium, CEC, 1996, pp. 329–334.
[9] F. Wittrock, R. Müller, A. Richter, H. Bovensmann, J.P. Burrows, Observations of Iodine monoxide above Spitsbergen, Geophys. Res. Lett. 27 (2000) 1471–1474.
[10] B. Alicke, K. Hebestreit, J. Stutz, U. Platt, Iodine oxide in the marine boundary layer, Nature 397 (1999) 572–573.
[11] B.J. Allan, G. McFiggans, J.M.C. Plane, H. Coe, Observation of iodine oxide in the remote marine boundary layer, J. Geophys. Res. 105 (2000) 14363–14370.
[12] A. Saiz-López, J.M.C. Plane, Novel iodine chemistry in the marine boundary layer, Geophys. Res. Lett. 31 (2004) L04112.
[13] R. Vogt, R. Sander, R. Von Glasow, P.J. Crutzen, Iodine chemistry and its role in halogen activation and ozone loss in the marine boundary layer: a model study, J. Atmos. Chem. 32 (1999) 375–395.
[14] G. McFiggans, J.M.C. Plane, B.J. Allan, L.J. Carpenter, H. Coe, C. O'Dowd, A modelling study of iodine chemistry in the marine boundary layer, J. Geophys. Res. 5 (D11) (2000) 14371–14385.
[15] B.J. Allan, J.M.C. Plane, G. McFiggans, Observations of OIO in the remote marine boundary layer, Geophys. Res. Lett. 28 (2001) 1945–1948.
[16] L.J. Carpenter, W.T. Sturges, S.A. Penkett, P.S. Liss, B. Alicke, K. Hebestreit, U. Platt, Short-lived alkyl iodides and bromides at mace head, Ireland: links to biogenic sources and halogen oxide production, J. Geophys. Res. 104 (D1) (1999) 1679–1689.
[17] R.J. Salawitch, Observations and Budgets of Minor constituents related to atmospheric ozone: an overview, in: Proceedings of the Quadrennial Ozone Symposium, 2004.
[18] David M. Rowley, J. William, R. Bloss, Anthony Cox, Roderic L. Jones, Kinetics and products of the IO + BrO reaction, J. Phys. Chem. A 105 (33) (2001) 7855–7864.
[19] T. Ingham, M. Cameron, J.N. Crowley, Photodissociation of IO (355 nm) and OIO (532 nm): quantum yields for O(^{3}P) and I(^{2}P$_J$) production, J. Phys. Chem. A 104 (2000) 8001–8010.
[20] S.H. Ashworth, B.J. Allan, J.M.C. Plane, High resolution spectroscopy of the OIO radical: implications for the ozone depleting potential of iodine, Geophys. Res. Lett. 29 (10) (2002) 1945–1948.
[21] J.N. Crowley, T.J. Dillon, D. Hölscher, A.M. Rodríguez, M.E. Tucceri, Photochemistry of IO and OIO, Geophys. Res. Abstr. 7 (2005) 04280.
[22] J. Plane, M. Joseph, S. Ashworth, R. Saunders, A. Saiz-López, A laboratory study of iodine chemistry in the atmosphere, Geophys. Res. Abstr. 7 (2005) 04893.

[23] U. Platt, Air monitoring by spectroscopic techniques, in: Chemical Analysis Series 127, Wiley, New York, 1994 (Chapter 2).
[24] W.M. Vaidya, The flame spectra of some aliphatic halides. Part I. (1) methyl iodide, Proc. Ind. Acad. Sci. 6A (1937) 122.
[25] E.H. Coleman, A.G. Gaydon, W.M. Vaidya, Spectrum of iodine oxide (IO) in flames, Nature (London) 162 (1948) 108–109.
[26] R.A. Durie, D.A. Ramsay, Absorption spectra of the halogen monoxides, Can. J. Phys. 36 (1958) 35–53.
[27] R.A. Durie, F. Legay, D.A. Ramsay, An emission system of the IO molecule, Can. J. Phys. 38 (1960) 444–452.
[28] R.A. Cox, G.B. Coker, Absorption cross section and kinetics of IO in the photolysis of CH_3I in the presence of ozone, J. Phys. Chem. 87 (1983) 4478–4484.
[29] M.E. Jenkin, R.A. Cox, Kinetics study of the reactions $IO + NO_2 + M \rightarrow IONO_2 + M$, $IO + IO \rightarrow$ products and $I + O_3 \rightarrow IO + O_2$, J. Phys. Chem. 89 (1985) 192–199.
[30] S.P. Sander, Kinetics and mechanism of the IO + IO reaction, J. Phys. Chem. 90 (1986) 2194–2199.
[31] R.E. Stickel, A.J. Hynes, J.D. Bradshaw, W.L. Chameides, D.D. Davies, Absorption cross sections and kinetic considerations of the IO radical as determined by laser flash photolysis/laser absorption spectroscopy, J. Phys. Chem. 92 (1988) 1862–1864.
[32] B. Lazlo, M.J. Kurylo, R.E. Huie, Absorption cross sections, kinetics of formation and self-reaction of the IO radical produced via the laser photolysis of $N_2O/I_2/N_2$ mixtures, J. Phys. Chem. 99 (1995) 11701–11707.
[33] M.H. Harwood, J.B. Burkholder, M. Hunter, R.W. Fox, A.R. Ravishankara, Absorption cross sections and self-reaction kinetics of the IO radical, J. Phys. Chem. A 101 (1997) 853–863.
[34] W.J. Bloss, D.M. Rowley, R.A. Cox, R.L. Jones, Kinetics and products of the IO self-reaction, J. Phys. Chem. A 105 (2001) 7840–7854.
[35] J. Tellinghuisen, Resolution of the visible-infrared absorption spectrum of I_2 into three contributing transitions, J. Chem. Phys. 58 (1973) 2821–2834.
[36] A. Saiz-Lopez, R.W. Saunders, D.M. Joseph, S.H. Ashworth, J.M.C. Plane, Absolute absorption cross-section and photolysis rate of I2, Atmos. Chem. Phys. 4 (2004) 1443–1450.
[37] P. Spietz, J.C. Gómez Martín, J.P. Burrows, Concentration dependent effects on I_2 reference spectra in the context of atmospheric DOAS and quantitative spectroscopy, Atmos. Chem. Phys. Disc. 5 (2005) 5183–5221.
[38] M.A.A. Clyne, H.W. Cruse, Rates of elementary reactions involving the BrO($X^2\Pi$) and IO($X^2\Pi$) radicals, Trans. Farad. Soc. 66 (1970) 2227–2236.
[39] J.C. Gómez Martín, P. Spietz, J. Orphal, J.P. Burrows, Principal and independent components analysis in the context of multichannel time resolved absorption spectroscopy, Spectrochim. Acta Part A 60 (2004) 2673–2693.
[40] P. Spietz, S. Himmelmann, U. Gross, J. Orphal, J.P. Burrows, Study of iodine oxides and iodine chemistry using flash photolysis and time resolved absorption spectroscopy, Ann. Geophys. Supp. II 16 (1998) C722.
[41] P. Spietz, J.C. Gómez Martín, J.P. Burrows, Spectroscopic studies of the I_2/O_3 photochemistry. Part 2. Improved spectra of iodine oxides and analysis of the io absorption spectrum 176 (2005) 50–67.
[42] A.T. Young, P.L. Houston, The $I(^2P_{1/2}) + O_2 \leftrightarrow I(^2P_{3/2}) + O_2(^1\Delta)$ equilibrium, J. Chem. Phys. 78 (5) (1983) 2317–2326.
[43] J. Shi, J.R. Barker, Kinetic studies of the deactivation of $O_2(^1\Sigma_g^+)$ and $O(^1D)$, Int. J. Chem. Kinet. 22 (1990) 1283–1301.
[44] K. Bogumil, J. Orphal, J.P. Burrows, Temperature dependent absorption cross sections of O_3, NO_2, and other atmospheric trace gases measured with the SCIAMACHY spectrometerdkjdot, in: Proceedings of ERS-Envisat Symposium 2000, ESA Publications Division, Göteborg, 2001.
[45] P. Spietz, U. Gross, E. Smalins, J. Orphal, J.P. Burrows, Estimation of the emission temperature of an electrodeless discharge lamp and determination of the oscillator strength for the $I(^2P_{3/2})$ 183.038 nm resonance transition, Spectrochim. Acta Part B 56 (2001) 2465–2478.
[46] C.W. Brown, P.F. Lynch, R.J. Obremski, D.S. Lavery, Matrix representations and criteria for selecting analytical wavelengths for multicomponent spectroscopic analysis, Anal. Chem. 54 (1982) 1472–1479.
[47] P. Spietz, J.C. Gómez Martín, J.P. Burrows, Quantitative treatment of insufficiently resolved and/or coarsely binned optical multichannel recordings in molecule absorption spectroscopy, Spectrochim. Acta Part A, in press.
[48] D.B. Atkinson, J.W. Hudgens, A.J. Orr-Ewing, Kinetic studies of the reactions of IO radicals determined by cavity ring-down spectroscopy, J. Phys. Chem. 103 (1999) 6173–6180.
[49] G. Inoue, M. Suzuki, N. Washida, Laser induced fluorescence of IO radicals and rate constant for the reaction IO + NO, J. Chem. Phys. 79 (10) (1983) 4730–4735.
[50] M.L.P. Rao, D.V.K. Rao, P.T. Rao, Dissociation energies, r-centroids and Franck–Condon factors of the IO molecule, Phys. Lett. 50A (5) (1974) 341–342.
[51] P. Spietz, J.C. Gómez Martín, U. Gross, E. Smalins, J. Orphal, J.P. Burrows, Atmospheric iodine chemistry: determination of the oscillator strength for the I(2P3/2) 183.038 nm resonance transition to be used for improved determination of IO and OIO cross sections, in: Proceedings of the 17th International symposium on gas kinetics, Essen (Germany), 2002.
[52] S.M. Newman, W.H. Howie, I.C. Lane, M.R. Upson, A.J. Orr-Ewing, Predissociation of the state $A^2\Pi_{3/2}$ of IO studied by cavity ring-down spectroscopy, J. Chem. Soc., Farad. Trans. 94 (1998) 2681–2688.
[53] G. Herzberg, Molecular Spectra and Molecular Structure. I. Spectra of Diatomic Molecules, Krieger Publishing Company, Malabar Florida, 1950.
[54] J.G. Calvert, J.N. Pitts, Photochemistry, John Wiley and Sons, New York, 1966.
[55] A.M. Malleson, H.M. Kellet, R.G. Myhill, W.P. Sweetenham (Eds.), FACSIMILE, AERE Harwell Publications, Oxfordshire, 1990.
[56] M.K. Gilles, A.A. Turnipseed, A.A. Talukdar, Y. Rudich, P.W. Villalta, L.G. Huey, J.B. Burkholder, A.R. Ravishankara, Reactions of $O(^3P)$ with alkyl iodides: rate coefficients and reaction products, J. Phys. Chem. 100 (100) (1996) 14005–14015.
[57] A. Mishra, P. Marshall, Computational investigations of iodine oxides, J. Phys. Chem. 102 (1998) 9056–9060.
[58] M.W. Chase, NIST-JANAF thermochemical tables for the iodine oxides, J. Phys. Chem. Ref. Data 25 (1996) 5.
[59] G. Maier, A. Bothur, Matrix isolation of iodine superoxide and iodine dioxide, Chem. Ber./Rec. 130 (1997) 179–181.
[60] V. Rozanov, A. Rozanov, R. de Beek, M. Buchwitz, D. Diebel, K.U. Eichmann, C. Haite, R.Hoogen, J. Kauss, T. Kurosu, J. Murray, R.J.D. Spurr, M. Vountas, J.P. Burrows, SCIATRAN 2.0.15, http://www.iup.uni-bremen.de/sciatran/index.html, Release date: 3 August, 2005.
[61] M. Buchwitz, K.U. Eichmann, A. Rozanov and J.P. Burrows, User's Guide for the Software Package SCIATRAN (Radiative Transfer Model and Retrieval Algorithm) -Version 2.0, http://www.iup.uni-bremen.de/sciatran/index.html, 2004.
[62] J.C. Gómez Martín, P. Spietz, J.P. Burrows, Reaction rates and mechanisms of product formation in the gas phase I_2/O_3 photochemistry, Geophys. Res. Abstr. 7 (2005) 01188.